ARTICLES

Metal Speciation Dynamics in Monodisperse Soft Colloidal Ligand Suspensions

Jérôme F. L. Duval,*,† José P. Pinheiro,‡ and Herman P. van Leeuwen§

Laboratory Environment and Mineral Processing, CNRS, Nancy-University, BP 40 - F-54501 Vandoeuvre-lès-Nancy Cedex, France, Centro de Biomedicina Molecular e Estrutural, Departamento de Quimica, Bioquimica e Farmácia, Faculdade de Ciencias e Tecnologia, Universidade do Algarve, Campus de Gambelas, 8005-139, Faro, Portugal, and Laboratory of Physical Chemistry and Colloid Science, Wageningen University, Dreijenplein 6, 6703 HB Wageningen, The Netherlands

Received: October 1, 2007; Revised Manuscript Received: April 3, 2008

A comprehensive theory is presented for the dynamics of metal speciation in monodisperse suspensions of soft spherical particles characterized by a hard core and an ion-permeable shell layer where ligands L are localized. The heterogeneity in the binding site distribution leads to complex formation/dissociation rate constants (denoted as k_a^* and k_d^*, respectively) that may substantially differ from their homogeneous solution counterparts (k_a and k_d). The peculiarities of metal speciation dynamics in soft colloidal ligand dispersions result from the coupling between diffusive transport of free-metal ions M within and around the soft surface layer and the kinetics of ML complex formation/dissociation within the shell component of the particle. The relationship between $k_{a,d}^*$ and $k_{a,d}$ is derived from the numerical evaluation of the spatial, time-dependent distributions of free and bound metal. For that purpose, the corresponding diffusion equations corrected by the appropriate chemical source term are solved in spherical geometry using a Kuwabara-cell-type representation where the intercellular distance is determined by the volume fraction of soft particles. The numerical study is supported by analytical approaches valid in the short time domain. For dilute dispersions of soft ligand particles, it is shown that the balance between free-metal diffusion within and outside of the shell and the kinetic conversion of M into ML within the particular soft surface layer rapidly establishes a quasi-steady-state regime. For sufficiently long time, chemical equilibrium between the free and bound metal is reached within the reactive particle layer, which corresponds to the true steady-state regime for the system investigated. The analysis reported covers the limiting cases of rigid particles where binding sites are located at the very surface of the particle core (e.g., functionalized latex colloids) and polymeric particles that are devoid of a hard core (e.g., polysaccharide macromolecules, gel particles). For both the transient and quasi-steady-state regimes, the dependence of $k_{a,d}^*$ on the thickness of the soft surface layer, the radius of the hard core of the particle, and the kinetic rate constants $k_{a,d}$ for homogeneous ligand solutions is thoroughly discussed within the context of dynamic features for colloidal complex systems.

1. Introduction

Nowadays, heavy metals are used in a large variety of industrial products such as paints (Pb, Cd), gasoline (Pb), and batteries (Pb, Cd, Ni, Zn), to quote only a few. As a result, the concentration level of a number of heavy metals in the environment has considerably increased, and much concern in environmental protection and health care policy has now arisen.[1–4] In aqueous media, metal ions are typically present over a broad range of complexes, resulting from their interaction with organic and inorganic chelating agents, for example, dissolved organic matter, dispersed colloidal particles, or microorganisms.[5] These binding entities largely differ in size, chemical composition, and structural anisotropy, thus leading to the formation of complexes with properties that vary significantly in terms of lability and bioavailability.[6] It is now well recognized that a scrupulous understanding of metal speciation is a mandatory prerequisite to quantitatively access the relationships between the various physicochemical forms of metals and their corresponding reactivity and mobility.[5] Because natural aquatic systems are never at equilibrium,[5] an appropriate formalism to account for their metal speciation should necessarily involve dynamic aspects. The latter stem from the interplay between kinetic features which underlie the interconversion of metal complex species in the bulk solution and transport processes of the relevant species (complex and metal) to/from the interface where species consumption (generally that of the free metal) takes place.

Until recently, the dynamic theories have entirely disregarded the discrete nature of the ligand distribution as typically met in colloidal dispersions. Instead, the complex formation/dissociation rate constants are commonly taken to be identical to those for homogeneous distribution of the available binding sites throughout the sample volume.[7–11] The shortcomings of such a simplistic approach have been recently underlined by Pinheiro

* To whom correspondence should be addressed.
† Nancy-University.
‡ Universidade do Algarve.
§ Wageningen University.

10.1021/jp709576j CCC: $40.75
Published on Web 07/17/2008

et al.,[12] who developed a formalism where steady-state complex formation/dissociation rate constants for colloidal ligand dispersions were defined taking into account the spatial confinement of the ligand sites to the very surface of the colloidal particles. Their theory was successfully supported by experimental measurements on lead and cadmium complexation by carboxyl-modified colloidal particles. In particular, it was shown that the formation/dissociation rate constants of complexes in colloidal dispersions and homogeneous ligand systems may differ by several orders of magnitude as a result of the differences in kinetic/mass-transport conditions. The major emerging feature is the evolution from a chemically kinetically controlled release of the metal to a diffusion-controlled one, which is intrinsically related to the dissimilarity in spatial ligand distributions.

Despite this breakthrough in our fundamental understanding of metal speciation dynamics in colloidal ligand systems, the treatment reported by Pinheiro et al.[12] is limited to the restrictive case of hard particles at the surface where ligands are located. In practice however, metal ions are generally present in dispersions of soft colloidal ligand particles[13] where binding sites are distributed according to three-dimensional spatial profiles. Polysaccharide macromolecules[14,15] and bacteria[16] are illustrative examples of such particles. To completely understand metal speciation dynamics in soft colloidal ligand systems, it is critical to quantitatively account for the distribution of free and bound metal within the particular volume where the ligands are distributed. This is essentially the purpose of the current work. We propose a rigorous theory that allows the evaluation of the time-dependent complex formation/dissociation rates in monodisperse suspensions of soft colloidal ligand particles with an arbitrary ratio between the core radius and surface layer thickness. As such, the dynamic model reported here covers the full spectrum of particle types, ranging from hard colloidal ligand to core/shell and polymeric (porous) particles. Also, the results shed some light on the nature of the steady-state regime for the dynamics of metal speciation in such soft colloidal ligand systems.

2. Theory

2.1. Geometrical Definitions and Formulation of the Problem. In the following, we consider a swarm of identical soft spherical particles of core radius a and shell thickness d (Figure 1A) dispersed in an aqueous medium where metal ions are present at an initial bulk concentration denoted as c_M^*. The ligands (L) are confined within the soft part of the particle at a constant, position-independent concentration denoted as c_L^*. The metal ion (M) can interact with the binding sites (L) to form the complex (ML) according to the reaction

$$M + L \underset{k_d}{\overset{k_a}{\rightleftharpoons}} ML \tag{1}$$

where k_a and k_d are the intrinsic complex formation and dissociation rate constants, respectively. The magnitude of the rate constant k_a is generally in agreement with the Eigen mechanism,[17] which comprises the formation of a precursor outer-sphere complex, with an electrostatically determined stability (K_{os}), followed by removal of water from the inner coordination sphere (k_w) as the usual rate-limiting step. The Eigen mechanism is applicable, provided that the impact of the electric field strength within the particle on k_a and k_d may be neglected, as assumed within the framework of the current study. The soft ligand particles are positioned according to a Kuwabara cell model representation[18] where each particle is considered to be surrounded by a virtual cell such that the particle/solution volume ratio in a unit cell equals the particle volume fraction for the entire system (Figure 1A). In the following, we denote the radius of the aforementioned unit cell as $a + r_c$, where r_c encompasses the soft surface layer thickness of the colloidal particle and that of the electrolyte solution distributed around it within the cell (Figure 1A). We thus have

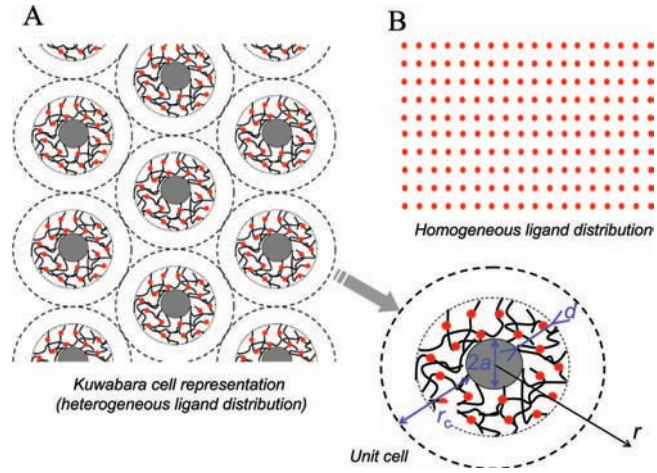

Figure 1. (A) Scheme (not to scale) of a dispersion of monodisperse soft colloidal ligand particles distributed according to a Kuwabara-cell-type representation. The unit cell of this representation is given with the indication of the nomenclature used for the coordinate system and for the geometrical parameters that define the particles. (B) Scheme of the situation where the distribution of molecular ligands is homogeneous throughout the sample volume. In panels A and B, the reactive sites (ligand) are indicated in red for the sake of readability.

$$r_c = (a + d)\phi^{-1/3} - a \tag{2}$$

or

$$r_c = (4\pi c_p/3)^{-1/3} - a \tag{3}$$

with ϕ as the particle volume fraction (hard core and soft components included) and c_p as the particle number concentration. Below, we shall assume that the position of the soft particles is "frozen" in time, which comes to consider cases where characteristic times of colloidal transport are infinitely long as compared to those relevant for the dynamics of molecular interaction between M and L. This simplification is generally legitimate for experimental systems of practical interest.[12,19,20] Besides, within the scope of the current analysis, we shall tackle the situation of unstirred aqueous media with a large excess of indifferent background electrolyte over the M species. This allows us to neglect the impact of the potential distribution related to double layer formation at the soft interface core/shell/aqueous solution on the free- and bound-metal concentration profiles within the unit cell. This is similar to the mathematical treatment encountered for microelectrodes.[21] The validity of this assumption is subject to the applicability of the relation $\kappa r_c \gg 1$, where κ represents the reciprocal screening Debye layer thickness. More quantitatively, neglect of the potential distribution within and outside of the particle is justified for electrostatic potential ψ that satisfies the inequality $\psi(r = a) \ll RT/F$ (where r is the radial position as indicated in Figure 1), with R as the gas constant, T as the temperature, and F as the Faraday. Therefore, to define the most restrictive value of $\psi(r = a)$ for validating the use of our model, we reason on the basis of the Donnan potential within the shell layer in the case of the uncharged core particle surface. Note that this is strictly valid for $\kappa d \gg 1$.[13] Then, after straightforward rearrangements,

we obtain the condition $\sinh^{-1}(\rho_{fix}/(2Fc^{\infty}|z|)) \ll 1$,[13] where ρ_{fix} is the volume charge density within the shell layer and c^{∞} is the bulk concentration of mobile ions with valence z (for the sake of simplicity, a z/z symmetrical background electrolyte is considered). With $|z| = 1$, this gives $(\rho_{fix}/Fc^{\infty}) \ll 2$. For $(\rho_{fix}/F) \sim 2-50$ mM, as found for functionalized carboxymethyldextran macromolecules[14] or bacteria,[13] we thus have $c^{\infty} \gg 1-25$ mM. Under the above conditions where conductive and convective metal transport to/from the reactive sites within the soft particle layer may be ignored, the conservation equations for the species M and ML within a unit cell are given by

$a < r < a + d$:

$$\begin{cases} \dfrac{\partial c_{ML}(r,t)}{\partial t} = -\{k_d c_{ML}(r,t) - k_a c_M(r,t) c_L^*\} \\ \dfrac{\partial c_M(r,t)}{\partial t} = D_M^p \nabla^2 c_M(r,t) + \{k_d c_{ML}(r,t) - k_a c_M(r,t) c_L^*\} \end{cases} \quad (4,5)$$

$$a + d < r < a + r_c: \quad \frac{\partial c_M(r,t)}{\partial t} = D_M^{sol} \nabla^2 c_M(r,t) \quad (6)$$

where $c_{i=M,ML}(r,t)$ is the local concentration of species i at a given time t and radial position r (the origin is taken at the center of the particle core) and $\nabla^2 \equiv \partial^2/\partial r^2 + (2/r)\partial/\partial r$ is the Laplacian operator in spherical geometry. The diffusion coefficients D_M^p and D_M^{sol} are those of free-metal species within and outside of the particle shell, respectively. For soft particles with sufficiently high water content, it is reasonable to assume the equality $D_M^p = D_M^{sol} = D_M$.[22-24] In other cases, the difference in magnitude between D_M^p and D_M^{sol} originates from steric and possibly electrostatic interactions between metal ions and ligand sites/polymer network.[23,24] The term in braces on the right-hand side of eqs 4 and 5 represents the chemical source term due to the association and dissociation of complex species. The tacit assumption that underlies the validity of eqs 4–6 is the consideration of excess binding sites as compared to free metal in solution, which comes to write the local ligand concentration $c_L(r,t)$ as $c_L(r,t) \approx c_L^* \gg c_M(r,t)$. In eqs 4 and 5, the transport of the L ligand or, for that matter, the ML complex within the shell layer is disregarded. This approximation is acceptable for particles with stiff and fairly immobile polymer chains that support the L reactive sites, which ensures inoperative motion of L/ML groups within the particle at the time scale pertaining to diffusive transport of M outside of the soft surface layer. Such approximation must be abandoned when examining metal speciation dynamics in soft ligand particles with highly flexible (charged) chains submitted to external fields, as within the framework of electrokinetic investigation or in dielectric spectroscopy. Those situations will be the subject of forthcoming analyses where metal speciation dynamics will be tackled in relation to dynamics of polymer chains, as intrinsically connected to their electrostatic and nanomechanical properties (e.g., elasticity). Note that L/ML movement is not necessarily random walk since reactive sites L are interconnected via polymer chains. For this reason, L/ML movement is not generally diffusive, and it is emphasized that it should be apprehended in connection with the dynamics of chains.

In colloidal ligand dispersions, the nonhomogeneous repartition of the binding sites within a unit cell that encloses a single particle (Figure 1A) may lead to reaction of M with L that is critically diffusion-limited (see eqs 5 and 6) as compared to the case where the ligand concentration is smeared out throughout the unit cell (Figure 1B). The purpose of the current paper is to determine the effective rate constants of complex formation/dissociation, denoted as k_a^* and k_d^*, respectively, that are physically relevant at the scale of the colloidal ligand system or, for that matter, at the scale of a unit cell as depicted in Figure 1A. The rate constants k_a^* and k_d^* should necessarily verify the conservation equations that are now written for a colloidal particle within a unit cell

$a < r < a + d$:

$$\begin{cases} \dfrac{\partial \rho_{ML}^V(t)}{\partial t} = -\{k_d^* \rho_{ML}^V(t) - k_a^* \rho_M^V(t) \rho_L^V\} \\ \dfrac{\partial \rho_M^V(t)}{\partial t} = D_M^p \nabla^2 \rho_M^V(t) + \{k_d^* \rho_{ML}^V(t) - k_a^* \rho_M^V(t) \rho_L^V\} \end{cases} \quad (7,8)$$

where the smeared-out concentrations $\rho_{i=M,L,ML}^V$ over the whole cell volume are defined by

$$i = M,L,ML: \quad \rho_i^V(t) = \frac{4\pi}{V_c} \int_a^{a+r_c} r^2 c_i(r,t) dr \quad (9)$$

with $V_c = 4\pi(a + r_c)^3/3 = c_p^{-1}$ as the volume of a unit cell and c_p as the particle number concentration introduced before. The determination of the constants k_a^* and k_d^* as a function of their molecular equivalents k_a and k_d will allow the identification of the physical operators that distinguish metal speciation dynamics in colloidal ligand suspensions from that in homogeneous solutions of ligands. To do so, it is critical to evaluate the time-dependent M and ML concentration profiles within a unit cell, which is done in the next section.

2.2. Concentration Profiles of Free and Bound Metal. Within the framework of the analysis, we do not a priori consider the presence of any consuming interfaces in the medium (i.e., electrode or microorganism). In such cases, the soft ligand particle finds itself in a macroscopic diffusion layer that is in contact with the metal-consuming interface. In section 3, the common aspects between this latter situation and that treated here (i.e., case of metal speciation dynamics in bulk dispersions of soft particles) will be discussed. The model developed below is necessarily valid within a given size window for the ligand particle for reasons that we now explicitly mention. The upper size limit is defined in relation with the fact that we exclude the impact of particle sedimentation on diffusive M transport. Indeed, large colloids may settle down with a time scale comparable to that of diffusion processes inside and outside of the particle and thereby affect the dynamics of kinetic/transport processes that govern metal speciation. Considering these elements, an upper size limit of about $1-10$ μm for the particle radius above which our results cannot be applied seems realistic. Also, the condition that underlies the neglect of movement of the particle on dynamics of the speciation processes of interest imposes $D_{particle} \ll D_M$, with $D_{particle}$ as the diffusion coefficient of the soft particle. If we consider the typical diffusion coefficient for M to be on the order of $5 \times 10^{-10}-10^{-9}$ m^2 s^{-1} and simply use the Stokes−Einstein equation for estimating the particle diffusion coefficient (with the criterion $D_{particle} = D_M/10$), we evaluate a lower size limit for the particle on the order of 2−5 nm. In addition, determination of the lower size limit should also include the size range where continuum transport modeling (adopted here) within the particle is valid. This imposes $l \ll d$, where l is the typical separation distance between two adjacent reactive sites. Taking $l \sim 0.5$ nm (as it is roughly the case for ionogenic sites along, e.g., a functionalized polysaccharide chain), we also come to $d \sim 5$ nm (if assuming $l/d \sim 10$ as sufficient to warrant application of continuum (fickian) transport theory).

This lower size limit (5 nm particle radius) corresponds to particles for which application of continuum models to derive transport or electrostatic properties remains debatable. Rigorous treatment for these types of particles would require advanced molecular computations of electrostatics and ion transport within/around the particles considered, which is well beyond the scope of the paper. It should be underlined that these molecular simulations are however not a panacea since they rely on prescribed intermolecular potentials which are, more often than not, difficult to justify at a quantum level.

The upper size limit of the model (1−10 μm particle radius) is basically that of microorganisms like bacteria. Metal speciation dynamics in living bacterial populations would require taking into account the inner flux due to biouptake by (or released from) the bacteria (e.g., via Michaelis−Menten-type of expression). Extension of the current model for such situations is straightforward, and it is stressed that the current model provides the fundamental basis for addressing these cases.

Given the above elements, our model is restricted to colloidal particles of radii in the range of 5 nm to 1−10 μm, for which spherical diffusion of metal ions may be regarded as the predominant mode of transport with a quickly achieved steady state.[19–21,25] In the following, we shall exclusively examine cases where $r_c \gg a$ and $r_c \gg d$ or, equivalently, where the dispersion of soft colloidal particles is sufficiently dilute so as to avoid the possible occurrence of significant overlap between diffusion layers that develop around two adjacent particles.[26] We stress however that the generality of the model proposed here allows for the examination of situations of concentrated particle suspensions. These will be explicitly analyzed in future communication where the impact of double layer effects on metal speciation dynamics in heterogeneous ligand distributions will also be considered. Below, the relevant spatial and temporal boundary conditions associated with eqs 4–6 are given. Then, the numerical theory for computing the M and ML concentration profiles within a unit cell is presented and further completed by analytical developments valid in the short time domain.

Boundary Conditions. At $t = 0$, the soft particles with ligands L are supposed to come into contact with aqueous solution that contains free-metal species M at initial bulk concentration c_M^*. The free- and bound-metal concentrations within the particle shell are set to zero, which gives

$$c_{ML}(a \le r \le a + d, t = 0) = 0 \tag{10}$$

$$c_M(a \le r \le a + d, t = 0) = 0 \tag{11}$$

while outside of the shell where there is necessarily no complex ML, we write

$$c_M(a + d \le r \le a + r_c, t = 0) = c_M^* \tag{12}$$

The required four spatial boundary conditions related to eqs 5 and 6 and associated with the concentration profile c_M within and outside of the soft surface layer are given by

$$\partial c_M(r, t)/\partial r|_{r=a,t} = 0 \tag{13}$$

$$\partial c_M(r, t)/\partial r|_{r=a+r_c,t} = 0 \tag{14}$$

$$c_M(r = a + d^-, t) = c_M(r = a + d^+, t) \tag{15}$$

and

$$D_M^p\, \partial c_M(r, t)/\partial r|_{r=a+d^-,t} = D_M^{sol} \partial c_M(r, t)/\partial r|_{r=a+d^+,t} \tag{16}$$

Equation 13 translates the impermeable character of the core particle surface for the free-metal species, and eq 14 stems from symmetry consideration for the M concentration profile at the position that corresponds to half of the separation distance between centers of two adjacent particles. Equations 15 and 16 reflect the continuity equations for M concentration and M flux at the edge of the soft surface layer, respectively. Note that the general boundary expressed by eq 14 simplifies into $c_M(r = a + r_c, t) = c_M^*$ for sufficiently dilute particle suspensions, that, is for $r_c \gg a + d$.

Numerical Analysis and Discretization of the Governing Equations 4–6, and 10–16. For the sake of mathematical and numerical convenience, we introduce the dimensionless variables

$$\tilde{t} = tD_M^p/pd^2 \tag{17}$$

$$k_{an} = k_a pd^2 c_L^*/D_M^p \tag{18}$$

$$k_{dn} = k_d pd^2/D_M^p \tag{19}$$

$$x_p = (r - a)/d \tag{20}$$

$$x_s = 1 + [r - (a + d)]/(r_c - d) \tag{21}$$

and

$$\tilde{c}_{M,ML}(r, t) = c_{M,ML}(r, t)/c_M^* \tag{22}$$

The parameter p in eq 17 is a nonzero scalar that allows adjustment of the time range of investigation for the dynamic processes of interest with $\tilde{t} \in [0,1]$. The scaled quantities x_p and x_s (eqs 20 and 21, respectively) satisfy the inequalities $0 \le x_p \le 1$ and $1 \le x_s \le 2$. They are further written

$$i = 1, ..., M: \quad x_{p,i} = (i - 1)\Delta x \tag{23}$$

$$i = 1, ..., M: \quad x_{s,i} = 1 + (i - 1)\Delta x \tag{24}$$

with M as an integer and $\Delta x = 1/(M - 1)$ as the spatial discretization step taken to be identical, for the sake of simplicity, in the r ranges that correspond to the shell and solution components of the unit cell of radius $a + r_c$. The dimensionless time $\tilde{t}$ is discretized according to

$$k = 1, ..., N: \quad \tilde{t}_k = (k - 1)\Delta t \tag{25}$$

with N as an integer and $\Delta t = 1/(N - 1)$ as the time discretization step. To lighten the notations, we define $\tilde{c}_{ML}(x_{p,i},\tilde{t}_k) = \tilde{c}_{ML\,i}^{\,k}$, $\tilde{c}_M(x_{p,i},\tilde{t}_k) = \tilde{c}_{M1\,i}^{\,k}$, and $\tilde{c}_M(x_{s,i},\tilde{t}_k) = \tilde{c}_{M2\,i}^{\,k}$. To optimize the convergence of the solution and reduce the computation time, eqs 4–6 and boundaries 10–16 are discretized following the "implicit backward Euler method".[27] Results are given in Appendix 1, where we show that the searched $\tilde{c}_{ML\,i}^{\,k}$, $\tilde{c}_{M1\,i}^{\,k}$, and $\tilde{c}_{M2\,i}^{\,k}$ are solutions of sets of linear equations written in matrix form as follows

$$k = 1, ..., N - 1: \quad \Omega \cdot \vec{C}^{(k+1)} = \vec{Q}^{(k)} \tag{26}$$

where Ω is a $3M \times 3M$ sparse matrix explicitly reported in Appendix 1, $\vec{C}^{(k+1)}$ and $\vec{Q}^{(k)}$ being column vectors defined by

$$k = 1, ..., N - 1: \quad \vec{C}^{(k+1)} = \left(\tilde{c}_{ML1}^{\,k+1}, ..., \tilde{c}_{MLM}^{\,k+1}, \tilde{c}_{M11}^{\,k+1}, ..., \tilde{c}_{M1M}^{\,k+1}, \tilde{c}_{M21}^{\,k+1}, ..., \tilde{c}_{M2M}^{\,k+1}\right)^T \tag{27}$$

and

$$\vec{Q}^{(k)} = \left(\tilde{c}_{ML1}^{\,k}, ..., \tilde{c}_{MLM}^{\,k}, 0, \tilde{c}_{M12}^{\,k}, ..., \tilde{c}_{M1M-1}^{\,k}, 0, 0, \tilde{c}_{M22}^{\,k}, ..., \tilde{c}_{M2M-1}^{\,k}, 0\right)^T \tag{28}$$

Let $\mathcal{F}$ be a numerical solver which enables the calculation of the components of the searched $\vec{C}^{(k+1)}$ from a known solution $\vec{C}^{(k)}$ and a given vector $\vec{Q}^{(k)}$, that is

$$k = 1, ..., N-1: \quad \vec{C}^{(k+1)} = \mathscr{T}(\vec{C}^{(k)}, \vec{Q}^{(k)}) \tag{29}$$

The column vector $\vec{C}^{(1)}$ corresponds to the situation at $\tilde{t} = 0$. From eq 27 and eqs 10–12, one easily shows that the only nonzero elements of $\vec{C}^{(1)}$ are given by $C^{(1)}_{i=2M+1,\ldots,3M} = 1$, where we choose the nomenclature $V_i^{(k)}$ to denote the ith component of any vector $\vec{V}^{(k)}$ ($\vec{V}^{(k)} \equiv \vec{C}^{(k)}$ or $\vec{V}^{(k)} \equiv \vec{Q}^{(k)}$). Using eqs 27 and 28, construction of the vector $\vec{Q}^{(1)}$ from $\vec{C}^{(1)}$ and, more generally, that of vector $\vec{Q}^{(k)}$ from $\vec{C}^{(k)}$ is straightforward. In particular, the nonzero elements of $\vec{Q}^{(1)}$ are given by $C^{(1)}_{i=2M+2,\ldots,3M} = 1$. Iterating k from 1 to $N-1$, with $\vec{C}^{(1)}$ as the starting solution previously defined, the vector $\vec{C}^{(k)}$ with the ML and M concentration profiles at time $\tilde{t}_k$ within the unit cell as components, can be evaluated. The numerical method subsumed in $\mathscr{T}$ for solving the linear algebraic sparse system (eq 26) with the right-hand side provided by the elements $Q_i^{(k)}$ is based on a LU decomposition of matrix Ω according to Crout's algorithm with partial pivoting.[27] The searched solution at time $\tilde{t}_k$ is subsequently obtained by classical combination of forward substitution and backsubstitution.[27] The accuracy and stability of the numerical solution was systematically verified by controlling the independence of the results on the quantities p, Δx, and Δt, with typical values for M and N around 1000 and 2000, respectively.

Analytical Approach. In this section, we derive analytical expressions for the concentration profiles of M and ML within a unit cell in the short domain. We shall see in section 3 that these analytical results are useful for reproducing dynamic data in transient and quasi-steady-state regimes as rigorously obtained from the numerical analysis detailed above. Within the framework of the analytical development below, it is convenient to introduce the functions $\xi_{ML}(\tilde{r},\hat{t})$ and $\xi_M(\tilde{r},\hat{t})$ defined by

$$\xi_{ML}(\tilde{r},\hat{t}) = r\tilde{c}_{ML}(\tilde{r},\hat{t}) \tag{30}$$

and

$$\xi_M(\tilde{r},\hat{t}) = r\tilde{c}_M(\tilde{r},\hat{t}) \tag{31}$$

where $\tilde{r} = (r-a)/r_c$ and $\hat{t} = D_M^{sol}t/r_c^2$. Note that, within the framework of the analytical approach, the scaled variable $\hat{t}$ differs from $\tilde{t}$ as considered for the numerical analysis. For very dilute particle suspensions with $r_c \to \infty$ (as exclusively examined in section 3), the particle shell thickness remains much thinner than the developing diffusion layer in solution, and the evolution of the concentrations of M and ML is largely determined by the shell filling process. It is hypothesized that for small $\hat{t}$, the time derivatives of the dimensionless concentrations $\tilde{c}_{M,ML}(\tilde{r},\hat{t})$ may be approximated by

$$\partial\tilde{c}_{M,ML}(\tilde{r},\hat{t})/\partial\hat{t} \approx [\tilde{c}_{M,ML}(\tilde{r},\hat{t}) - \tilde{c}_{M,ML}(\tilde{r},\hat{t}=0)]/\hat{t} \tag{32}$$

which will be shown to work satisfactorily for dilute systems over a broad time range t by comparing analytical and numerical results. For concentrated suspensions, the applicability of eq 32 is expected to pertain to a more restricted time range t, thereby recalling that eq 32 is rigorous for $\hat{t} \to 0$. We mention here analogous treatments in refs 28–30 for obtaining approximate analytical solutions (see details below) to problems that involve complicated partial differential equations. Using eqs 10–12 and eqs 30–32, eqs 4–6 then reduce to

$$0 < \tilde{r} < \tilde{d}: \begin{cases} \xi_{ML}(\tilde{r},\hat{t})\left(1+\tilde{k}_d\hat{t}\right) - \tilde{k}_a\hat{t}\xi_M(\tilde{r},\hat{t}) = 0 \\ \varepsilon\dfrac{\partial^2\xi_M(\tilde{r},\hat{t})}{\partial\tilde{r}^2} + \tilde{k}_d\xi_{ML}(\tilde{r},\hat{t}) - \dfrac{1+\tilde{k}_a\hat{t}}{\hat{t}}\xi_M(\tilde{r},\hat{t}) = 0 \end{cases} \tag{33,34}$$

$$\tilde{d} < \tilde{r} < 1: \quad \frac{\partial^2\xi_M(\tilde{r},\hat{t})}{\partial\tilde{r}^2} - \lambda(\hat{t})^2\{\xi_M(\tilde{r},\hat{t}) - r_c(\tilde{r}+\tilde{a})\} = 0 \tag{35}$$

where $\tilde{d} = d/r_c$, $\tilde{a} = a/r_c$, $\varepsilon = D_M^p/D_M^{sol}$, $\lambda(\hat{t})^2 = 1/\hat{t}$, $\tilde{k}_a = k_a r_c^2 c_L^*/D_M^{sol}$ and $\tilde{k}_d = k_d r_c^2/D_M^{sol}$. Substitution of $\xi_{ML}(\tilde{r},\hat{t})$ as obtained from eq 33 into eq 34 leads to

$$0 < \tilde{r} < \tilde{d}: \quad \frac{\partial^2\xi_M(\tilde{r},\hat{t})}{\partial\tilde{r}^2} - \beta(\hat{t})^2\xi_M(\tilde{r},\hat{t}) = 0 \tag{36}$$

with

$$\beta(\hat{t})^2 = [1 + (\tilde{k}_a + \tilde{k}_d)\hat{t}]/[\varepsilon\hat{t}(1+\tilde{k}_d\hat{t})] \tag{37}$$

Integration of eqs 35 and 36 is straightforward. The results read as

$$\tilde{d} < \tilde{r} < 1: \quad \xi_M(\tilde{r},\hat{t}) = C_1(\hat{t})\cosh[\lambda(\hat{t})\tilde{r}] + C_2(\hat{t})\sinh[\lambda(\hat{t})\tilde{r}] + r_c(\tilde{r}+\tilde{a}) \tag{38}$$

$$0 < \tilde{r} < \tilde{d}: \quad \xi_M(\tilde{r},\hat{t}) = C_3(\hat{t})\cosh[\beta(\hat{t})\tilde{r}] + C_4(\hat{t})\sinh[\beta(\hat{t})\tilde{r}] \tag{39}$$

where $C_{1,2,3,4}(\hat{t})$ are time-dependent integration constants. Boundary conditions given by eqs 13 and 14 are expressed in terms of ξ_M by the relationships

$$\tilde{a}\left.\frac{\partial\xi_M(\tilde{r},\hat{t})}{\partial\tilde{r}}\right|_{\tilde{r}=0} - \xi_M(\tilde{r}=0,\hat{t}) = 0 \tag{40}$$

and

$$(1+\tilde{a})\left.\frac{\partial\xi_M(\tilde{r},\hat{t})}{\partial\tilde{r}}\right|_{\tilde{r}=1} - \xi_M(\tilde{r}=1,\hat{t}) = 0 \tag{41}$$

respectively. The continuity eqs 15 and 16 at the edge of the soft surface layer are rewritten

$$\xi_M(\tilde{r}=\tilde{d}^-,\hat{t}) = \xi_M(\tilde{r}=\tilde{d}^+,\hat{t}) \tag{42}$$

and

$$\varepsilon(\tilde{a}+\tilde{d})\left.\frac{\partial\xi_M(\tilde{r},\hat{t})}{\partial\tilde{r}}\right|_{\tilde{r}=\tilde{d}^-} = (\tilde{a}+\tilde{d})\left.\frac{\partial\xi_M(\tilde{r},\hat{t})}{\partial\tilde{r}}\right|_{\tilde{r}=\tilde{d}^+} - (1-\varepsilon)\xi_M(\tilde{r}=\tilde{d}^-,\hat{t}) \tag{43}$$

respectively. The complete determination of the concentration profiles c_{ML} and c_M, or equivalently ξ_{ML} and ξ_M, requires the evaluation of the integration constants $C_{1,2,3,4}(\hat{t})$ from eqs 38–43. Full derivation of $C_{1,2,3,4}(\hat{t})$ is given in Appendix 2 (eqs A31–A34 therein). The set of eqs 33, 38, 39, and A31–A34 rigorously defines the concentration profiles of M and ML over the relevant space regions, that is, within the soft part of the colloidal ligand particle and in the electrolyte solution around it. In Appendix 2, simplified expressions for $C_{1,2,3,4}(\hat{t})$ are provided in the limit of dilute particle suspensions, that is, for $c_p \ll 1$ or equivalently $r_c \to \infty$ (that limit is strictly examined in section 3 within the framework of the current analysis). We underline that the quantities $\beta(\hat{t})\tilde{r}$, $\lambda(\hat{t})\tilde{r}$, $\tilde{k}_d\hat{t}$, and $\tilde{k}_a\hat{t}$ entering

the expressions of local M and ML concentration profiles are all independent of r_c.

2.3. Complex Formation−Dissociation Rate Constants for Discrete Soft Colloidal Ligand Systems. The integration of both sides of eq 4 over the volume of the soft surface layer leads to

$$\frac{\partial \rho^{s}_{ML}(t)}{\partial t} = -k_d \rho^{s}_{ML}(t) + k_a \rho^{s}_{M}(t) c^{*}_{L} \tag{44}$$

where we have introduced the smeared-out concentrations $\rho^{s}_{i=M,ML}$ over the shell layer volume of the particle as follows

$$i = M, ML: \quad \rho^{s}_{i}(t) = \frac{4\pi}{V_s}\int_{a}^{a+d} r^2 c_i(r,t)\mathrm{d}r \tag{45}$$

with $V_s = 4\pi\{(a+d)^3 - a^3\}/3$ as the volume over which the reactive binding sites L are distributed. Multiplication of both sides of eq 44 by the ratio V_s/V_c leads to

$$\frac{\partial \rho^{V}_{ML}(t)}{\partial t} = -k_d \rho^{V}_{ML}(t) + k_a \rho^{s}_{M}(t) \rho^{V}_{L} \tag{46}$$

where we recall that $\rho^{s}_{L} = c^{*}_{L}$ and

$$i = L, ML: \quad \rho^{V}_{i}/\rho^{s}_{i} = V_s/V_c \tag{47}$$

The tacit assumption that leads to the derivation of eq 46 is that the reaction rate constants $k_{a,d}$ that pertain to homogeneous ligand systems (Figure 1B) also hold within the volume reaction layer V_s. This simplification was introduced and justified in the treatment proposed by Pinheiro et al.[12] for the limiting case of steady-state metal speciation dynamics in hard colloidal ligand systems. It comes to ignore the impact of the interconnection between the binding sites, via the polymer chain network within the soft part of the colloidal particle, on the reactivity of the individual ligand species. In other words, the intrinsic rate of formation of a metal complex in an aqueous shell layer is considered to be basically the same as that in bulk solution. Following this, we may write that the equilibrium constants for local and homogeneous ligand concentrations[12] are identical, that is

$$\frac{k^{*}_{a}}{k^{*}_{d}} = \frac{k_a}{k_d} = K \tag{48}$$

where K is the stability constant of the ML complex. In Appendix 3, the validity of this expression for any time t is demonstrated. For entirely porous particles ($a \rightarrow 0$) in a macroscopic diffusion layer at a consuming interface (e.g., electrode), Zhang et al.[31] also pointed out that it is always possible to formally write the pertaining rate constants, denoted as k^{**}_{a} and k^{**}_{d} (which a priori differ from $k^{*}_{a,d}$ due to the presence of the macroscopic diffusion layer), as $k^{**}_{a} = G(t)k_a$ and $k^{**}_{d} = G(t)k_d$, where $G(t)$ is a function of time. The searched rate constants $k^{*}_{a,d}$ of interest here are necessarily verifying eq 7. Eliminating the time derivative terms between eqs 7 and 46 and using eq 48, one obtains the general relationship between k^{*}_{a} and k_a

$$\frac{k^{*}_{a}(t)}{k_a} = \frac{\rho^{s}_{M}(t)\rho^{V}_{L} - \rho^{V}_{ML}(t)K^{-1}}{\rho^{V}_{M}(t)\rho^{V}_{L} - \rho^{V}_{ML}(t)K^{-1}} \tag{49}$$

where the time dependences of ρ^{s}_{M}, ρ^{V}_{M}, ρ^{V}_{ML}, and k^{*}_{a} have been written explicitly. A similar expression may be derived for the ratio k^{*}_{d}/k_d. For a given time t, the determination of the required ρ^{s}_{M}, ρ^{V}_{M}, and ρ^{V}_{ML} was carried out by numerical integration (according to Simpson's rule[27]) of the corresponding cubic spline interpolated concentrations as evaluated from the $\tilde{c}_{MLi}{}^{k}$, $\tilde{c}_{M1i}{}^{k}$, and $\tilde{c}_{M2i}{}^{k}$ obtained by a finite-elements algorithm. In the short time domain, explicit expression for k^{*}_{a}/k_a may be derived using the analytical profiles $c_{M,ML}(r,t)$ and $C_{1,2,3,4}(t)$ given in eqs 33, 38, 39, and A31–A34. Details of the latter derivation are available in Appendix 4. After rearrangements, the analytical expression for the ratio k^{*}_{a}/k_a for $t \rightarrow 0$ as a function of the key kinetic, transport, and geometric parameters reads as

$$\frac{k^{*}_{a}(\hat{t})}{k_a} = \frac{(V_s c_p)^{-1}\rho^{V}_{L} - K^{-1}\dfrac{\tilde{k}_a \hat{t}}{1+\tilde{k}_d\hat{t}}}{\rho^{V}_{L}\left[1 + \dfrac{\dfrac{V_c - V_p}{4\pi} + \left(\dfrac{r_c}{\lambda(\hat{t})}\right)^2 C_1(\hat{t})h_2(\hat{t})}{\left(\dfrac{r_c}{\beta(\hat{t})}\right)^2 C_4(\hat{t})h_1(\hat{t})}\right] - K^{-1}\dfrac{\tilde{k}_a\hat{t}}{1+\tilde{k}_d\hat{t}}} \tag{50}$$

where the general expressions of the time-dependent functions $C_{1,4}(\hat{t})$ and $h_{1,2}(\hat{t})$ are given in Appendix 2 (eqs A31 and A34) and Appendix 4 (eqs A59 and A60), respectively. V_p in eq 50 denotes the volume of the particle, core and shell included. Straightforward simplifications of eq 50 for $r_c \rightarrow \infty$ may be done taking into account $(V_c - V_p) \sim (c_p)^{-1}$ and the limiting expressions of $C_{1,4}(\hat{t})$ and $h_2(\hat{t})$ for $r_c \rightarrow \infty$ given in Appendices 2 and 4 (eqs A39, A42, and A61). Note that the quantities $(r_c/\lambda(\hat{t}))^2$ and $(r_c/\beta(\hat{t}))^2$ in eq 50 are independent of r_c.

3. Results and Discussion

3.1. Concentration Profiles of M and ML and Typical Time Dependence for k^{*}_{a}/k_a. To quantify the differences in metal speciation dynamics between discrete colloidal ligand suspensions and homogeneous ligand solutions, we first report in Figure 2A,B the concentration profiles of free M and bound ML metal species within and/or outside of the soft surface layer with ligands. Results are given for different snapshots in time as obtained from the numerical evaluation (eqs 26–29 and Appendix 1) of the governing time-dependent reaction−diffusion equations (eqs 4–6) under appropriate boundary conditions (eqs 10–16). Before commenting on these results, it is emphasized that all calculations reported here are consistent, for the sake of convenience and comparison, with the condition that the smeared-out ligand concentration, ρ^{V}_{L}, is kept constant over the entire range of time, a, or d/a values examined. This implies that the particle number concentration c_p varies according to the relationship $c_p = \rho^{V}_{L}/(V_s c^{*}_{L})$ that directly follows from eq 47 for i = L. The value of ρ^{V}_{L} considered in this paper is further in agreement with the necessary conditions $\tilde{a} \ll 1$ and $\tilde{d} \ll 1$ (r_c being evaluated from eq 3) or equivalently $\phi \ll 1$.

Starting from the situation at $t = 0$ where M and ML species are absent from the particle shell, ML concentration at a given position within the shell continuously increases with time as a result of gradual diffusion of free M from the solution (outside of the particle) to the reactive shell layer and subsequent complexation. In doing so, the ML concentration at fixed time decreases from $r = a + d$ to $r = a$, the highest ML concentration being located at the position $r = a + d$, that is, the surface that the free metal has to cross to yield ML. The decrease in the ML concentration from the outer edge of the soft surface layer to the very interface core/shell is related to the corresponding decrease in free-metal concentration as governed by the differ-

ences in the chemical potential of free M species outside of and within the shell (diffusive transport). For sufficiently long time, ML and M concentration gradients within/outside of the shell are significantly reduced, and local equilibrium within the soft particle surface layer is reached. The latter situation simply corresponds to local chemical equilibrium associated with the reaction in eq 1, that is

$$\frac{c_{ML}(r,t)}{c_L^* c_M(r,t)} \rightarrow K \qquad (51)$$

For $t \rightarrow \infty$, M and ML concentration profiles are flat, and eq 51 simply becomes $c_{ML}/(c_L^* c_M) = K$ with $c_M = c_M^*$. It is then verified that the constant K corresponds to the ratio $\rho_{ML}^V/(\rho_L^V \rho_M^V)$ (see eq 7 in the steady sate and eq 48) as numerically computed for $t \rightarrow \infty$ (agreement with less than 0.1% error). That the steady-state regime for the processes of interest here corresponds to trivial chemical equilibrium within the whole shell is straightforwardly inferred from eqs 4–6 solved in the limit $\partial c_{ML,M}(r,t)/\partial t = 0$. This simple treatment further confirms the results of Figure 2 obtained for sufficiently long time t, in particular, that the concentration profile of free M satisfies at every position $r \geq a$ the relation $\tilde{c}_M(r,t) \rightarrow 1$.

Figure 2C illustrates the time dependence of the ratio k_a^*/k_a (eq 49) under the conditions of Figure 2A,B. Close examination of this dependence in relation with the M and ML concentration profiles commented above reveals the existence of three distinct regimes in the dynamics of the processes that govern metal speciation in soft colloidal ligand suspensions. The first regime corresponds to the short time limit and reflects the dynamically developing M diffusion layer around the particle (see Figure 2B): the transient regime. Just for orientation, we give the simple expression for the dynamic diffusion-controlled flux, denoted as J_{diff}, for free M toward/from a colloidal particle of radius $a + d$

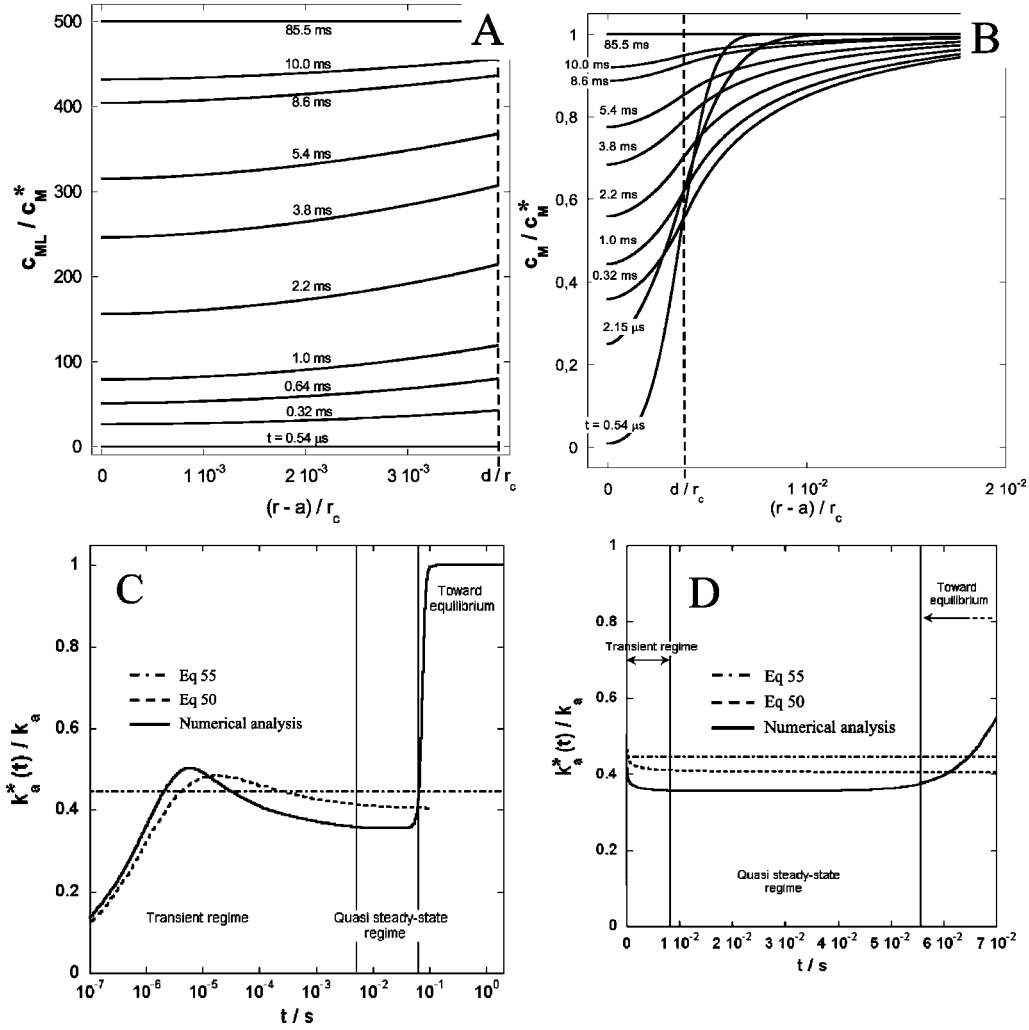

Figure 2. (Panel A) Normalized concentration profiles of complex species ML within the soft shell layer of the particle where the reactive sites L are located. (Panel B) Normalized concentration profiles of free-metal M within and outside of the soft shell layer of the particle. Results are given for different times, as explicitly indicated, and were obtained from the numerical analysis detailed in the text. To avoid figure overcharge, the situation at $t = 0$ is not depicted ($\tilde{c}_M(r > a + d, t = 0) = 1$, $\tilde{c}_{M,ML}(a < r < a + d, t = 0) = 0$). For the sake of clarity, the position that corresponds to the interface between the outer edge of the particle shell and the solution is marked with a dotted line (position $r = a + d$ or equivalently $\tilde{r} = \tilde{d} = d/r_c$). (Panel C) Time dependence of the ratio $k_a^*(t)/k_a$ as obtained from numerical analysis (eqs 26–29, and 49 and Appendix 1) from the approximate eq 50 valid in the short time domain and from time-independent eq 55 that neglects the M and ML concentration polarization within the shell. In the inset (Panel D), a zoom of the time variation of $k_a^*(t)/k_a$ in the quasi-steady-state regime where the curve meaning is identical to that in Panel C. Model parameters for Figure 2: $a = 20$ nm, $d = 100$ nm, $D_M = 9.85 \times 10^{-10}$ m^2 s^{-1}, $c_L^* = 10^{-2}$ mol m^{-3}, $\rho_L^V = 10^{-9}$ mol m^{-3}, $T = 298$ K, $K = 5 \times 10^4$ mol^{-1} m^3, $k_w = 7 \times 10^9$ s^{-1}, and $K_{os} = 3.66 \times 10^{-3}$ mol^{-1} m^3. The values of D_M and k_w pertain to Pb(II) metal ion (ionic strength 0.01 M)[12] while that of K is typical of metal complexation by carboxylate groups distributed at the surface of latex particles.[12] The value of ρ_L^V considered in Figure 2 is in agreement with the condition $\tilde{a} \ll 1$ and $\tilde{d} \ll 1$ or equivalently $\phi \ll 1$.

$$J_{\text{diff}} = D_{\text{M}}\Delta c_{\text{M}}\{(\pi D_{\text{M}}t)^{-1/2} + (a+d)^{-1}\} \qquad (52)$$

where Δc_{M} is the driving concentration difference. In the situation analyzed here, Δc_{M} evolves with time. The $(\pi D_{\text{M}}t)^{-1/2}$ term in eq 52 stands for linear diffusion, and the term $(a + d)^{-1}$ accounts for the sphericity of diffusion. The transient regime physically corresponds to a time domain where J_{diff} is a function of time, that is, for t from zero to t for which $(\pi D_{\text{M}}t)^{1/2} \gg a + d$. For soft particles of radius in the range of 5 nm to 5 μm where our formalism may be applied (see discussion in section 2.2), this yields time windows of O(100 ns)−O(0.1s). This estimation is done with a D_{M} of O(10^{-9}m^2 s^{-1}) and taking the criterion $(\pi D_{\text{M}}t)^{1/2} = 10(a + d)$ for evaluating the critical time that marks the arbitrary boundary between transient and steady- or quasi-steady-state regimes (see below). In the initial stage of the transient regime, we have $k_{\text{a}}^*(t \to 0)/k_{\text{a}} \to 0$ in line with eq 49 and the boundaries in eqs 10 and 11, which lead to $\rho_{\text{ML}}^{\text{V}}(t \to 0) \to 0$ and $\rho_{\text{M}}^{\text{s}}(t \to 0) \to 0$, respectively. When increasing time, $k_{\text{a}}^*(t)/k_{\text{a}}$ increases as a result of the accumulation of M and ML within the shell layer. After some time, $k_{\text{a}}^*(t)/k_{\text{a}}$ decreases, which is reflected in the presence of a maximum. This maximum is due to a slight decrease of $\rho_{\text{M}}^{\text{s}}(t)$ as intrinsically related to the gradual building up of the M diffusion layer at both sides of the very interface between the shell layer and electrolyte solution (see Figure 2B,D). As shown later (Figure 3), this maximum is absent for cases where $k_{\text{a}}^*(t)/k_{\text{a}} \to 1$, that is, when the process is rate-limited essentially by the kinetics of the reaction in eq 1.

In the light of Figure 2C (or Figure 2D, where $k_{\text{a}}^*/k_{\text{a}}$ is plotted as a function of time according to linear axis representation), a second regime may be identified. It follows the transitory establishment of M diffusion profile, and it is characterized by a nearly constant $k_{\text{a}}^*/k_{\text{a}}$: the quasi-steady-state regime. In this regime where important time variations are observed for the local M and ML concentrations (Figure 2), it can be readily shown that the numerically obtained M concentration profiles for $r \geq a + d$ may be approximated by

$$r \geq a + d: \quad c_{\text{M}}(r,t) \approx \{c_{\text{M}}(r = a + d, t) - c_{\text{M}}^*\}\frac{a+d}{r} + c_{\text{M}}^* \qquad (53)$$

which is the steady-state profile for diffusion-limited (M) species outside of the shell. The flux J_{diff} of M from or toward the particle (eq 52) then maintains its steady-state nature, that is

$$J_{\text{diff}}(t) = D_{\text{M}}\left.\frac{\partial c_{\text{M}}(r,t)}{\partial r}\right|_{r=a+d} \approx D_{\text{M}}\Delta c_{\text{M}}(t)/(a+d) \qquad (54)$$

with $\Delta c_{\text{M}}(t) = c_{\text{M}}^* - c_{\text{M}}(r = a + d, t)$. Given eq 54, it can be easily shown (details of the derivation are reported in Appendix 5) that $k_{\text{a}}^*/k_{\text{a}}$ may be then approximated by

$$k_{\text{a}}^*/k_{\text{a}} \approx \left(1 + \frac{k_{\text{a}}\rho_{\text{L}}^{\text{V}}}{4\pi(a+d)D_{\text{M}}c_{\text{p}}}\right)^{-1} \qquad (55)$$

which is independent of time. Comparison of $k_{\text{a}}^*/k_{\text{a}}$ as obtained from numerical analysis and from eq 55 (Figure 2D) confirms the acceptable validity of eqs 53 and 54 in the quasi-steady-state regime for the dynamic processes analyzed here. The observed discrepancies in the example of Figure 2 arise from the approximations that underlie the derivation of eq 55, mainly the neglect of concentration polarization of M and ML within the shell layer (see details in Appendix 5). As such, eq 55 may be viewed as a first-order expression for $k_{\text{a}}^*/k_{\text{a}}$ in the quasi-steady-state regime.

For sufficiently long time t, the third regime, already invoked above, is that where local M and ML concentrations are those dictated by eq 51 (local chemical equilibrium). On the basis of eqs 9 and 45, for zero gradients of M and ML concentration distributions within and/or outside of the particle (situation at $t \to \infty$), we directly obtain

$$t \to \infty: \quad \rho_{\text{M}}^{\text{V}} = \rho_{\text{M}}^{\text{s}} = c_{\text{M}}^* \quad \text{and} \quad \frac{k_{\text{a}}^*}{k_{\text{a}}} = 1 \qquad (56,57)$$

Equation 57 results from combining eq 56 with eq 49. In the

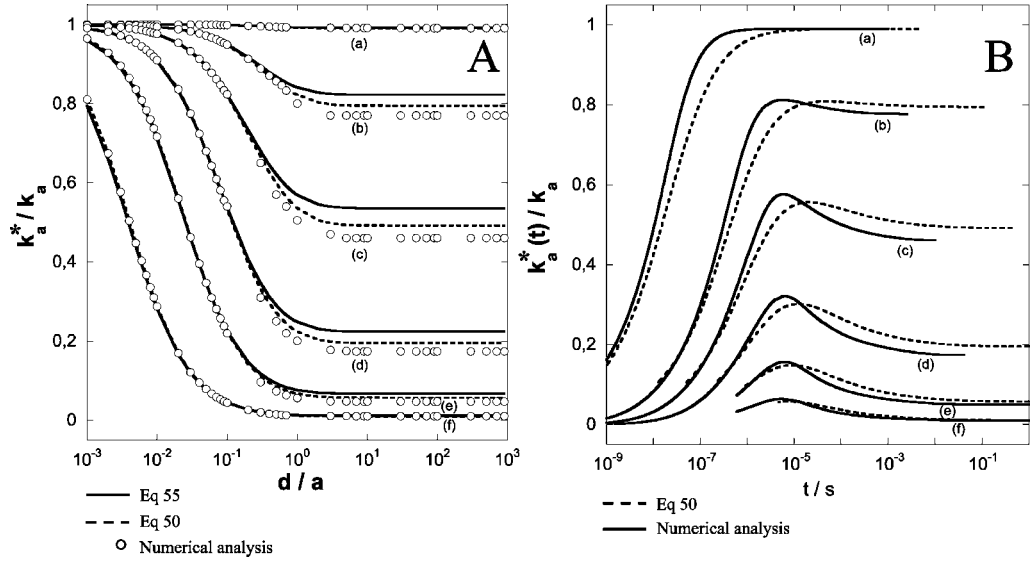

Figure 3. (Panel A) Ratio $k_{\text{a}}^*/k_{\text{a}}$ in the time range that corresponds to the quasi-steady-state regime as a function of d/a under the condition $a + d$ = constant: (a) $a + d = 10$ nm, (b) 50 nm, (c) 100 nm, (d) 200 nm, (e) 400 nm, and (f) 1 μm. The open circles pertain to $k_{\text{a}}^*/k_{\text{a}}$ as evaluated from numerical analysis (eqs 26–29, and 49 and Appendix 1), the dashed lines refer to $k_{\text{a}}^*/k_{\text{a}}$ obtained from eq 50, while the plain lines correspond to eq 55 (see text for further detail). Other model parameters as those in Figure 2. (Panel B) Time dependence of the ratio $k_{\text{a}}^*(t)/k_{\text{a}}$ in the transient and quasi-steady-state regimes under the conditions of Panel A with $d/a = 10^3$. Plain lines: numerical analysis (eqs 26–29, and 49 and Appendix 1). Dashed lines: eq 50 valid in the short time domain. All computations pertain to very dilute suspensions of colloidal ligand particles ($r_{\text{c}} \gg a + d$) of which the volume fraction ϕ is easily obtained via $\phi = \rho_{\text{L}}^{\text{V}}(c_{\text{L}}^*)^{-1}(1 - [1 + d/a]^{-3})^{-1}$ (which results from the combination of eqs 23 and 47 (i = L)).

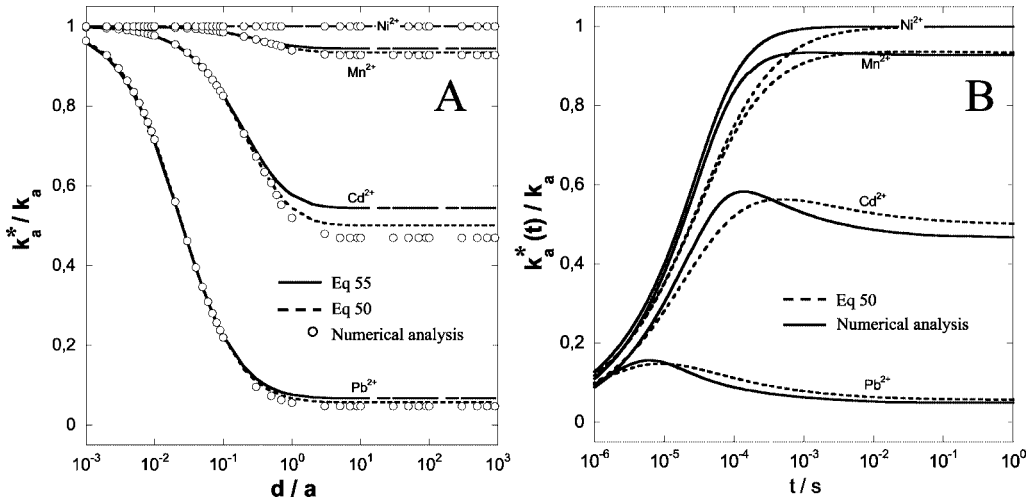

Figure 4. (Panel A) Ratio k_a^*/k_a in the time range that corresponds to the quasi-steady-state regime as a function of d/a for $a + d = 400$ nm for lead(II), cadmium(II), manganese(II), and nickel(II) (indicated). The open circles refer to the k_a^*/k_a obtained from numerical analysis (eqs 26–29, and 49 and Appendix 1), the dashed lines to k_a^*/k_a obtained from eq 50, while the plain lines correspond to eq 55 (see text for further detail). Other model parameters are as those in Figure 2 except $D_{Pb} = 9.85 \times 10^{-10}$ m^2 s^{-1}, $D_{Cd} = 7 \times 10^{-10}$ m^2 s^{-1}, $D_{Mn} = D_{Ni} = 1 \times 10^{-9}$ m^2 s^{-1}; $k_w(Pb) = 7 \times 10^9$ s^{-1}, $k_w(Cd) = 3 \times 10^8$ s^{-1}, $k_w(Mn) = 3 \times 10^7$ s^{-1}, and $k_w(Ni) = 3 \times 10^4$ s^{-1}, which are tabulated values extracted from ref 12 (0.01 M ionic strength and $z_M z_L = -2$ with z_M and z_L as the valence of M and L, respectively). The choice $a = 400$ nm is in agreement with the particle size window where the model is applicable. It is recalled that according to Eigen,[17] $k_a = K_{os}k_w$. (Panel B) Time-dependence of the ratio $k_a^*(t)/k_a$ in the transient and quasi-steady-state regimes under the conditions of Panel A with $d/a = 10^3$. Plain lines: numerical analysis (eqs 26–29, and 49 and Appendix 1). Dashed lines: eq 50 valid in the short time domain.

regime where local chemical equilibrium prevails (eq 51), following the reasoning above, we have for increasing time a ratio k_a^*/k_a, which increases and gradually reaches the value 1, in agreement with Figure 2C and eq 57. In Figure 2C,D, the time dependence of k_a^*/k_a as obtained from the analytical expression given by eq 50 (valid for short time) is reported together with that evaluated from eq 55 (quasi-steady-state approximation) and the "exact" numerical solution to the key dynamic transport equations. The first comment is that the general features of the dependence of k_a^*/k_a on time are well reproduced by eq 50 (initial increase of k_a^*/k_a, presence of a maximum, and setting of a quasi-steady-state regime). In the transient and especially in the quasi-steady-state regime ($t \leq 0.06$s or $\hat{t} \leq 0.09$ under the condition of Figure 2), eq 50 provides a very good first-order estimate for the numerically evaluated k_a^*/k_a (Figure 2D). The slight differences between the two stem from the approximation expressed by eq 32, which constitutes the starting step in the analytical approach that leads to eq 50. In the following, the discrepancy between the general formation rate constant k_a^* and its counterpart for homogeneous ligand solution, k_a, are discussed in detail within the context of dynamic features for colloidal complex systems.

3.2. Impact of Colloidal Ligand Particle Dimensions on Metal Speciation Dynamic Features. In Figure 3, we report the dependence of k_a^*/k_a in the quasi-steady-state regime (cf. section 3.1) on the shell−core ratio, d/a, for various values of the particle radius $a + d$, in agreement with the size window discussed in section 2.2 where our model is applicable. For the sake of comparison, results derived from the "exact" numerical analysis (eqs 26–29, and 49 and Appendix 1) and those from the approximate eqs 50 and 55 are all collected. It is here recalled that the results are presented for variation of the ratio d/a and/or $a + d$ at constant smeared-out ligand concentration, ρ_L^V (with $\phi \ll 1$). This condition is satisfied via the change of the particle number concentration c_p according to $c_p = \rho_L^V/(V_s c_L^*)$. The strong variations of k_a^*/k_a with d/a under the conditions of Figure 3 (or Figure 4) are not governed by the corresponding variations of c_p (providing $\phi \ll 1$) as imposed by the condition of constant ρ_L^V. This is straightforwardly verified by rewriting eq 55 in the form $k_a^*/k_a \approx (1 + k_a V_s c_L^*/4\pi(a + d)D_M)^{-1}$, where the impact of the geometrical parameters of the particle are explicitly indicated, recalling that $V_s = 4\pi\{(a + d)^3 - a^3\}/3$. It is anticipated that variation of c_p will be critical in the examination of the impact of electrostatics on metal speciation dynamics by soft colloids (study currently in preparation). Indeed, such variation will lead to changes of r_c which, if comparable to a few times the double layer thickness, will in turn generate modulations of the interfacial electric field and thus of the M transport characteristics and ultimately of k_a^*/k_a. From Figure 3, it is noted that the generalized formation rate constant of the complex ML, k_a^*, may differ from k_a by several orders of magnitude, particularly for soft colloidal ligand particles characterized by large particle radius $a + d$ and/or significant surface layer thickness, that is, $d/a \gg 1$. Under such conditions where $k_a^*/k_a \ll 1$, metal speciation in colloidal ligand systems is rate-limited by the diffusive transport of free-metal ions to/from the soft surface layer that contains the binding sites. In the other limiting situation where k_a^*/k_a approaches unity, the rate of the overall process is determined by the kinetics of the reaction in eq 1. For ligand particles of given $a + d$, we note that the ratio k_a^*/k_a as evaluated from numerical analysis is correctly reproduced by the approximate eqs 50 and 55, even if some deviations are observed particularly for cases where $k_a^*/k_a \sim 0.5$. In more detail, it is observed that the merging between the rigorous k_a^*/k_a and those obtained from eqs 50 and 55 at given $a + d$ is excellent for low values of d/a (typically $d/a < 1$), while some discrepancies show up for $d/a > 1$. These are understood by arguing that (i) the time delay required to reach quasi-steady-state regime increases upon increase of the shell thickness (Figure 3B), thus rendering eq 50 (based on the approximation in eq 32) less accurate, and (ii) the concentration polarization of M and ML within the shell becomes more significant for increasing thickness of the particle surface layer, which makes eq 55 more approximate upon increase of $a + d$ and d/a, except for the particle geometry, such that k_a^*/k_a reaches the limiting values 0 or 1. Figure 3 illustrates the fundamental

difference in dynamic features of metal speciation by hard and entirely porous colloidal ligand particles, which corresponds to the situations where $d/a \ll 1$ and $d/a \gg 1$, respectively. Considering the situation where k_a is sufficiently large for appreciating the full range of dynamic features when varying d/a, for cases where $d/a \gg 1$, metal speciation is significantly rate-limited by the diffusive transport of the free-metal ions, which corresponds to decreasing values of k_a^*. In situations where $d/a \ll 1$, the rate of interconversion of M into ML within the volume reaction where binding sites are located controls predominantly the dynamics of the processes: the nonequilibrium regime governed by chemical kinetics. For intermediate values of d/a, coupling between the kinetic determinants of the reaction in eq 1 (i.e., the constants $k_{a,d}$) and the diffusive transport of free metal to/from the soft surface layer comes into play. Figure 3 underlines the incorrectness when assimilating a soft porous ligand particle to a hard sphere. Note that such assimilation is (unfortunately) still common in other fields of colloidal science like electrokinetics, as extensively commented in ref 13. It is emphasized that the expression in eq 50 provides an excellent estimate of the ratio k_a^*/k_a not only in the quasi-steady-state regime but also in the transient where the M diffusion layer gradually develops around the ligand particle.

We underline the strong analogy between the physical operators that govern metal speciation dynamics in bulk suspensions of soft colloidal ligand particles, as extensively analyzed here, and that in suspensions of ligand particles that find themselves in a macroscopic diffusion layer. To deepen this analogy, let us first consider the simple scheme of a metal ion M that associates with a soft colloidal ligand particle and an interface which acts as a sink for free metal. This interface may be an electrode or a consuming biointerface like a microorganism. Complex systems are called static if they are unable to restore equilibrium at the relevant time scale t of the experiment, whereas they are considered dynamic if equilibrium is fully maintained across the macroscopic diffusion layer, that is, the rates for the volume reactions are fast on the relevant time scale of the experiment, as mathematically expressed by eq 58 below. As commented in ref 12, the two limits of static and dynamic colloidal complexes in the presence of a consuming interface should be written by replacing in the conventional dynamic criteria for metal complex the commonly used rate constants $k_{a,d}$ for homogeneous solution of ligands by their generalized forms, denoted as $k_{a,d}^{**}$

$$\text{For dynamic complex (ML):} \quad k_d^{**}t, k_a^{**}\rho_L^V t >> 1 \tag{58}$$

$$\text{For static complex (ML):} \quad k_d^{**}t, k_a^{**}\rho_L^V t << 1 \tag{59}$$

The contribution of dynamic colloidal metal complexes to an overall metal flux at a given electrode or microorganism interface is governed by the magnitude of the macroscopic diffusive flux as compared to that of the macroscopic kinetic flux. We then speak of labile (diffusion control) or nonlabile (kinetic control) metal complexes. In a previous analysis by Pinheiro et al.,[12] $k_{a,d}^{**}$ were derived as a function of $k_{a,d}$ for hard colloidal ligand particles ($d/a \ll 1$) under "steady-state" conditions using an analytical formalism based on a coarse-grained representation of individual particles placed in the vicinity of a consuming interface. Their result reads

$$k_{a,d}^{**}/k_{a,d} \approx \left(1 + \frac{k_a \rho_L^V}{4\pi a D_M c_p}\right)^{-1} \tag{60}$$

In a more recent study by Zhang and co-workers,[31] the expressions of $k_{a,d}^{**}$ for entirely porous particles (devoid of hard core, $a = 0$) located in a macroscopic diffusion layer were derived. Their "steady-state" treatment, done via the numerical evaluation of Laplace transforms of the M and ML concentration profiles within and outside of the porous particle, was found to be in agreement, within a few percent error, with the similar expression

$$k_{a,d}^{**}/k_{a,d} \approx \left(1 + \frac{k_a \rho_L^V}{4\pi d D_M c_p}\right)^{-1} \tag{61}$$

Comparing eq 60 with eq 61 leads us to conclude that the effective kinetic constants $k_{a,d}^{**}$ for the situation of hard or porous colloidal complexes in a large-scale diffusion layer with a thickness that well exceeds the size of the particle do not depend on the free- and bound-metal concentration polarization within the reactive layer of the particle. Within the framework of the current analysis (absence of consuming interface), we have shown that the expression in eq 55, which basically considers M and ML concentrations as constant within the shell (Appendix 5), generally yields a satisfactory estimate for the numerically evaluated $k_{a,d}^*$ over the entire spectrum of dynamic situations with values of k_a^*/k_a ranging from 1 for $d/a \ll 1$ to 0 for $d/a \gg 1$ even if deviations are more pronounced for cases where $d/a \gg 1$, as explained above. Equations 60 and 61 are nothing else than the limits of eq 55 for $d/a \ll 1$ and $d/a \gg 1$, respectively. In the analyses reported in refs 12 and 31, the local and coarse-grained governing transport equations for M and ML within and outside of the shell are equivalent to those considered here, written with a Kuwabara cell representation under the condition $r_c \rightarrow \infty$. Given this, the true "steady state" for these cases is that explicitly indicated in this manuscript, that is, the trivial chemical equilibrium, as directly inferred from solution of the corresponding equations for $\partial c_{ML,M}(r,t)/\partial t = 0$. With these elements in mind, the similarity in the quasi-steady-state regime (which precedes the setting of chemical equilibrium) between dynamics of metal speciation in suspensions of colloidal ligand particles in the presence and absence of a macroscopic diffusion layer is explained by the fact that in both situations, the time variation of the ML concentration over the shell volume may be related to the steady-state gradient of the M concentration profile at the outer edge of the shell, that is

$$\frac{\partial}{\partial t}\{\rho_{ML}^V(t) + V_s c_p \rho_M^s(t)\} \approx 4\pi(a+d)D_M c_p\{c_M^* - c_M(r=a+d,t)\} \tag{62}$$

which results from the combination of eq 54 with the volume integration of the sum of eqs 4 and 5 using the relationship (see details in Appendix 5)

$$\int_a^{a+d} r^2 \nabla^2 c_{ML}(r,t)\mathrm{d}r = (a+d)^2 \left.\frac{\mathrm{d}c_{ML}}{\mathrm{d}r}\right|_{r=a+d} \tag{63}$$

Note that eq 62, valid for any core−shell particle, is the three-dimensional generalization of the expression given in ref 12 for the time variation of complex surface concentration in the case of hard colloidal ligand particles. Using eq 62 in relation with eq 46, neglecting the spatial details of the M concentration distribution within the shell (i.e., $\rho_M^s(t) \approx c_M(r = a + d, t)$) and writing $\rho_M^V(t) \approx c_M^*$ for $r_c \rightarrow \infty$, one obtains the general expression in eq 55 valid for any core−shell particle, from hard to porous types (cf. details in Appendix 5). In view of the discussion above, we state that under quasi-steady-state conditions

$$k_{a,d}^{**} = k_{a,d}^{*} \quad (64)$$

and that eqs 58 and 59 also hold for the situation of metal speciation dynamics in bulk suspensions of soft colloidal ligand particles.

3.3. Impact of $k_{a,d}$ on Metal Speciation Dynamics. For the sake of completeness, Figure 4A shows the dependence of k_a^*/k_a in the quasi-steady-state regime on the ratio d/a for $a + d =$ 400 nm and various trace metals (Pb, Cd, Mn, and Ni) characterized by similar diffusion coefficients D_M ($\sim 10^{-9}$ m^2 s^{-1}) and significantly different intrinsic complex formation rate constants, k_a. The first observation is that the larger the k_a, the lower the k_a^*/k_a for a given d/a. This is so because deviation of k_a^* from k_a is most important when metal speciation is critically limited by the diffusion process, or said differently, the kinetics of interconversion of M into ML is fast (large k_a, dynamic case). The results depicted in Figure 4 highlight that a dynamic system for homogeneously distributed molecular ligands (condition $k_d t$, $k_a c_L^* t \gg 1$, which is the pendent of eq 58 for homogeneous ligand solution) may be less dynamic when the L reactive sites are confined within a colloidal shell because, in essence, $k_a^*/k_a < 1$. Finally, the time dependence of $k_a^*(t)/k_a$ in the transient and quasi-steady-state regime is given in Figure 4B under the condition of Figure 4A with $d/a = 10^3$. As in Figure 3B, the analytical expression for $k_a^*(t)/k_a$ given by eq 50 satisfactorily reproduces the exact numerical results over the whole range of time that pertains to the transient and quasi-steady-state regime. Upon increase of k_a, that is, from Ni(II) to Pb(II), the strong diffusion limitation for the inner/outer flux of free M outside of the particle shell leads to a dramatic decrease of k_a^*/k_a, which reflects very different properties of the colloidal complex in terms of dynamics (eqs 58 and 59). Whereas the assimilation of $k_{a,d}^*$ to $k_{a,d}$ is appropriate for Ni(II), it is unacceptable for metal ions with faster kinetic reactions (i.e., larger k_a) with significantly diffusion-limited speciation.

4. Conclusions

We propose a theory for the quantitative account of metal speciation dynamics in bulk dispersions of core−shell colloidal ligand particles ranging from hard ($d/a \ll 1$) to porous ($d/a \gg 1$) types. The proposed model is based on the numerical evaluation of the time-dependent concentration distributions of free and bound metal within (M and ML) and outside (only M) of the soft ligand particles distributed according to a Kuwabara cell representation. The M and ML concentration profiles are derived by consistent numerical analysis of the coupled kinetic and diffusive-transport equations of M and ML within and/or outside of the volume reaction layer of the particle where reactive sites are located. Following this, we derive a general time-dependent expression for the kinetic complex formation/dissociation rate constants ($k_{a,d}^*$) in colloidal ligand dispersions as a function of their pendents for homogeneous ligand distributions ($k_{a,d}$) and the integrals of M and ML concentrations over the shell and unit cell volumes. The numerical computation of these and thus of $k_{a,d}^*$ is supported by (i) an analytical theory, valid in the short time domain, which reproduces satisfactorily the dynamic features of metal speciation by soft particles in the transient and particularly quasi-steady-state regime and (ii) an analytical expression for $k_{a,d}^*$ under quasi-steady-state conditions, which satisfactorily coincides with that obtained from rigorous numerical estimation. Our analysis has far-reaching implications for the dynamic features of soft colloidal metal complexes and their lability with respect to interfacial processes. It is basically demonstrated that the dynamics of metal speciation in soft particle suspensions located or not within a macroscopic diffusion layer (which stems from the presence of a consuming interface like an electrode or microorganism) are similar in the quasi-steady-state regime where a gradient of the M concentration at the outer edge of the shell particle maintains its steady-state nature. As such, our analyses extend the approach developed in refs 12 and 31 for hard and soft colloidal particles, respectively, and quantitatively explains the impact of the M and ML concentration polarization within the particle shell layer on $k_{a,d}^*$. The role of the geometrical parameters that define the soft particles and that of the intrinsic complex formation/dissociation rate constants $k_{a,d}$ are discussed in detail. In forthcoming analyses, we will extend our approach for investigating the dynamics of metal speciation in soft colloidal ligand particles in relation with the dynamically developing interfacial double layer within and outside of the shell particle. This will provide the sound theoretical ground for capturing the spectral signature of dynamic colloid−metal interaction processes as measured by dielectric spectroscopy (AC electrokinetics). Such analysis is essential to understand the impact of metal−soft colloid binding on the electrodynamics of the soft particles of interest. It is thereby expected to provide new insight, for example, into the dynamics of coagulation processes mediated by inter/intramolecular bridging between soft constituents of colloids and metals. In conjunction with that, the impact of bulk metal depletion on the ratio $k_{a,d}^*/k_{a,d}$ as a result of the evolving overlap between diffusion layers of neighboring particles will be critically examined and so will the impact of electric double layer field (at the interface particle/solution) on metal speciation dynamics. Overlap between adjacent diffusion layers (~few microns scale) and electric double layers (~few nanometers scale) is of importance for colloidal ligand particle dispersions of a sufficiently high volume fraction and sufficiently low salinity, respectively, as possibly encountered in practical systems. Finally, it is emphasized that the analysis reported here may be straightforwardly adapted to capture the basics of dynamics of nutrients/pollutants uptake and/or release by bacteria, which are paradigms of soft (bio)colloids.

Acknowledgment. The authors thank two anonymous referees for their valuable comments in their rebuttals to this work.

Appendix 1. Discretization of the Governing Equations 4–6 and Corresponding Boundaries from Equations 10–16

For a given time $\tilde{t}_k$, discretization of eqs 4–6 following the implicit backward Euler method yields

$$i = 1, ..., M: \quad (1 + k_{dn}\Delta t)\tilde{c}_{MLi}^{\,k+1} - k_{an}\Delta t\tilde{c}_{M1i}^{\,k+1} = \tilde{c}_{MLi}^{\,k} \quad (A1)$$

$$i = 2, ..., M-1: \quad \alpha_{M1}(i)\tilde{c}_{M1i}^{\,k+1} + \beta_{M1}(i)\tilde{c}_{M1i+1}^{\,k+1} - p(\Delta t/\Delta x^2)\tilde{c}_{M1i-1}^{\,k+1} - k_{dn}\Delta t\tilde{c}_{MLi}^{\,k+1} = \tilde{c}_{M1i}^{\,k} \quad (A2)$$

and

$$i = 2, ..., M-1: \quad \alpha_{M2}(i)\tilde{c}_{M2i}^{\,k+1} + \beta_{M2}(i)\tilde{c}_{M2i+1}^{\,k+1} - \omega(\Delta t/\Delta x^2)\tilde{c}_{M2i-1}^{\,k+1} = \tilde{c}_{M2i}^{\,k} \quad (A3)$$

where $\omega = D_M^s pd^2/[D_M^p(r_c - d)^2]$ and $\alpha_{M1,2}(i)$ and $\beta_{M1,2}(i)$ are provided by

$$i = 2, ..., M-1: \quad \alpha_{M1}(i) = 1 + 2p\Delta t\{1/\Delta x^2 + 1/[\Delta x(x_{p,i} + a/d)] + k_{an}/(2p)\} \quad (A4)$$

$$i=2,...,M-1:\quad \alpha_{M2}(i)=$$
$$1+2\omega\Delta t\left\{1/\Delta x^2+1/\left[\Delta x\left(x_{s,i}-1+\frac{a+d}{r_c-d}\right)\right]\right\} \quad (A5)$$

$$i=2,...,M-1:\quad \beta_{M1}(i)=$$
$$-(p\Delta t/\Delta x^2)\{1+2\Delta x/(x_{p,i}+a/d)\} \quad (A6)$$

$$i=2,...,M-1:\quad \beta_{M2}(i)=$$
$$-(\omega\Delta t/\Delta x^2)\left\{1+2\Delta x/\left(x_{s,i}-1+\frac{a+d}{r_c-d}\right)\right\} \quad (A7)$$

The finite differences equations associated with the boundaries of eqs 13–16 for a given time $\tilde{t}_{k+1}$ are given by

$$\tilde{c}_{M12}^{\,k+1}-\tilde{c}_{M11}^{\,k+1}=0 \quad (A8)$$

$$\tilde{c}_{M2M}^{\,k+1}-\tilde{c}_{M2M-1}^{\,k+1}=0 \quad (A9)$$

$$\tilde{c}_{M1M}^{\,k+1}-\tilde{c}_{M21}^{\,k+1}=0 \quad (A10)$$

and

$$\sigma\left(\tilde{c}_{M1M}^{\,k+1}-\tilde{c}_{M1M-1}^{\,k+1}\right)=\tilde{c}_{M22}^{\,k+1}-\tilde{c}_{M21}^{\,k+1} \quad (A11)$$

respectively. The quantity σ in eq A11 is defined by $\sigma = D_M^p(r_c - d)/(D_M^{sol}d)$. Eqations A1–A3 and A8–A11 may be formally written in the matrix form provided by eqs 26–28 in the main text with the $3M \times 3M$ sparse matrix Ω of which the nonzero elements are defined by

$$i=1,...,M:\quad \begin{cases}\Omega(i,i)=(1+k_{dn}\Delta t)\\ \Omega(i,i+M)=-k_{an}\Delta t\end{cases} \quad (A12, A13)$$

$$\Omega(M+1,M+1)=-1 \qquad \Omega(M+1,M+2)=1 \quad (A14, A15)$$

$$i=M+2,...,2M-1:\quad \begin{cases}\Omega(i,i-M)=-k_{dn}\Delta t\\ \Omega(i,i-1)=-p(\Delta t/\Delta x^2)\\ \Omega(i,i)=\alpha_{M1}(i-M)\\ \Omega(i,i+1)=\beta_{M1}(i-M)\end{cases} \quad (A16-A19)$$

$$\begin{cases}\Omega(2M,2M-1)=-\sigma\\ \Omega(2M,2M)=\sigma\\ \Omega(2M,2M+1)=1\\ \Omega(2M,2M+2)=-1\end{cases} \quad (A20-A23)$$

$$\Omega(2M+1,2M)=1 \qquad \Omega(2M+1,2M+1)=-1 \quad (A24, A25)$$

$$i=2M+2,...,3M-1:\quad \begin{cases}\Omega(i,i-1)=-\omega(\Delta t/\Delta x^2)\\ \Omega(i,i)=\alpha_{M2}(i-2M)\\ \Omega(i,i+1)=\beta_{M2}(i-2M)\end{cases} \quad (A26-A28)$$

$$\Omega(3M,3M-1)=-1 \qquad \Omega(3M,3M)=1 \quad (A29, A30)$$

Note that the elements of the matrix Ω correspond to those of the Jacobian associated with the set of linear equations given by eqs A1–A3 and A8–A11. It is important to emphasize here that the numerical computation of the M and ML concentration profiles can be considerably faster by considering exclusively the spatial range outside of the particle shell where nonzero gradients for the M concentration are encountered. This comes to reduce the range of x_s values to the interval $[1,d(\theta - 1)/(r_c - d)]$, with $\theta > 1$ defined as the scalar for which $\partial c_M(r,t)/\partial r|_{r=a+\theta d,t} = 0$. Adopting such a strategy imposes replacing in eqs A3, A5, A7, and A26 the quantities Δx and Δx^2 by $d\Delta x(\theta - 1)/(r_c - d)$ and $\{d\Delta x(\theta - 1)/(r_c - d)\}^2$, respectively and replacing the right-hand sides of eqs A22 and A23 by $(r_c - d)/[d(\theta - 1)]$ and $-(r_c - d)/[d(\theta - 1)]$, respectively.

Appendix 2. Expressions for the Integration Constants $C_{1,2,3,4}(\hat{t})$

The integration constants $C_{1,2,3,4}(\hat{t})$, which enter the definition of the concentration profiles for M and ML within the unit cell of radius $a+r_c$ (eqs 30, 31, 33, 38, and 39), are determined by the set of four boundary conditions expressed by eqs 40–43. After proper combination of eqs 38, 39, and 40–43, one may show that the $C_{1,2,3,4}(\hat{t})$ are solutions of a linear set of equations written

$$C_1(\hat{t})=\{(a+d)f_3(\hat{t})-\varepsilon r_e f_4(\hat{t})\}\left\{f_4(\hat{t})\left[\lambda(\hat{t})\sinh(\lambda(\hat{t})\tilde{d})-\frac{1-\varepsilon}{\tilde{a}+\tilde{d}}\cosh(\lambda(\hat{t})\tilde{d})-\frac{f_1(\hat{t})}{f_2(\hat{t})}\left[\lambda(\hat{t})\cosh(\lambda(\hat{t})\tilde{d})-\frac{1-\varepsilon}{\tilde{a}+\tilde{d}}\sinh(\lambda(\hat{t})\tilde{d})\right]\right]-f_3(\hat{t})\left[\cosh(\lambda(\hat{t})\tilde{d})-\frac{f_1(\hat{t})}{f_2(\hat{t})}\sinh(\lambda(\hat{t})\tilde{d})\right]\right\}^{-1} \quad (A31)$$

$$C_2(\hat{t})=-\frac{f_1(\hat{t})}{f_2(\hat{t})}C_1(\hat{t}) \quad (A32)$$

$$C_3(\hat{t})=\tilde{a}\beta(\hat{t})C_4(\hat{t}) \quad (A33)$$

with

$$C_4(\hat{t})=\frac{1}{f_4(\hat{t})}\left\{C_1(\hat{t})\left[\cosh(\lambda(\hat{t})\tilde{d})-\frac{f_1(\hat{t})}{f_2(\hat{t})}\sinh(\lambda(\hat{t})\tilde{d})\right]+a+d\right\} \quad (A34)$$

The time-dependent functions $f_{1,2,3,4}(\hat{t})$ are provided by

$$f_1(\hat{t})=\lambda(\hat{t})(1+\tilde{a})\sinh(\lambda(\hat{t}))-\cosh(\lambda(\hat{t})) \quad (A35)$$

$$f_2(\hat{t})=\lambda(\hat{t})(1+\tilde{a})\cosh(\lambda(\hat{t}))-\sinh(\lambda(\hat{t})) \quad (A36)$$

$$f_3(\hat{t})=\varepsilon\beta(\hat{t})[\cosh(\beta(\hat{t})\tilde{d})+\tilde{a}\beta(\hat{t})\sinh(\beta(\hat{t})\tilde{d})] \quad (A37)$$

and

$$f_4(\hat{t})=\sinh(\beta(\hat{t})\tilde{d})+\tilde{a}\beta(\hat{t})\cosh(\beta(\hat{t})\tilde{d}) \quad (A38)$$

respectively. Given that, for any $\tilde{r}$ and $\hat{t}$, $\beta(\hat{t})\tilde{r}$, $\lambda(\hat{t})\tilde{r}$, $\tilde{k}_d\hat{t}$, and $\tilde{k}_a\hat{t}$ are all independent of r_c, eqs A31–A34 simplify in the limit $r_c \rightarrow \infty$ as follows

$$C_1(\hat{t})=\left\{\varepsilon\frac{r_c}{\beta(\hat{t})}f_4(\hat{t})-(a+d)\frac{f_3(\hat{t})}{\beta(\hat{t})}\right\}\times\left\{[\cosh(\lambda(\hat{t})\tilde{d})-\sinh(\lambda(\hat{t})\tilde{d})]\left[\frac{f_3(\hat{t})}{\beta(\hat{t})}+f_4(\tilde{t})\left(\frac{\lambda(\hat{t})}{\beta(\hat{t})}+\frac{1-\varepsilon}{\beta(\hat{t})[\tilde{a}+\tilde{d}]}\right)\right]\right\}^{-1} \quad (A39)$$

$$C_2(\hat{t})=-C_1(\hat{t}) \quad (A40)$$

$$C_3(\hat{t})=\tilde{a}\beta(\hat{t})C_4(\hat{t}) \quad (A41)$$

with

$$C_4(\hat{t}) = \frac{1}{f_4(\hat{t})}\{C_1(\hat{t})[\cosh(\lambda(\hat{t})\tilde{d}) - \sinh(\lambda(\hat{t})\tilde{d})] + a + d\} \quad \text{(A42)}$$

It may be straightforwardly verified that the functions $f_3(\hat{t})\beta(\hat{t})^{-1}$, $r_c\beta(\hat{t})^{-1}$, and $\lambda(\hat{t})\beta(\hat{t})^{-1}$ introduced in eq A39 are independent of r_c.

Appendix 3. Demonstration of the Relationship $k_a^*/k_d^* = k_a/k_d = K$

Let us assume that $\rho_M^s(t)$ may be written in the form

$$\rho_M^s(t) = g_1(t)\rho_M^V(t) + [1 - g_1(t)]g_2(t) \quad \text{(A43)}$$

where g_1 and g_2 are functions of time to be determined. Let us further write

$$\partial\rho_{ML}^V(t)/\partial t = g_3(t)[\rho_M^V(t) - g_2(t)] \quad \text{(A44)}$$

with g_3 as a third function of time to be derived in the following. Then, elimination of $g_2(t)$ between eqs A43 and A44 and substitution of the resulting expression for $\rho_M^s(t)$ into eq 46 leads to

$$\frac{\partial\rho_{ML}^V(t)}{\partial t} = -\frac{k_d}{1 + k_a\rho_L^V\dfrac{1 - g_1(t)}{g_3(t)}}\rho_{ML}^V(t) + \frac{k_a}{1 + k_a\rho_L^V\dfrac{1 - g_1(t)}{g_3(t)}}\rho_M^V(t)\rho_L^V \quad \text{(A45)}$$

Identifying eq A45 with eq 7 immediately demonstrates that in the equilibrium situation where $\partial\rho_{ML}^V(t)/\partial t = 0$, we have $k_a^*/k_d^* = k_a/k_d = K$, which is eq 48 in the main text. The question remains whether it is effectively possible to determine the functions g_1, g_2, and g_3. We show below that it is the case. Prior to this, we mention in Appendix 4 that the time dependences of ρ_M^s, ρ_M^V, and ρ_{ML}^V are explicitly derived in the short time domain and that the time dependence of these functions or their derivatives with respect to time (at any t) may be rigorously obtained from the numerical analysis of the M and ML concentration profiles as detailed in the text. Given these elements, we now determine for the sake of illustration g_1, g_2, and g_3 in the short time domain, but demonstration for any time t may be carried out along the same lines on the basis of the numerically computed concentration profiles and thus of the related functions ρ_M^s, ρ_M^V, and ρ_{ML}^V. Combination of eqs A55 and A57 (given in Appendix 4) provides

$$\rho_{ML}^V(t) = Q(t)[\rho_M^V(t) - R(t)] \quad \text{(A46)}$$

with $Q(t) = \tilde{k}_a\hat{t}/(1+\tilde{k}_d\hat{t})$ and

$$R(t) = \frac{4\pi r_c^2 c_M^*}{V_c}\int_{\tilde{d}}^1 (\tilde{r} + \tilde{a})\xi_M(\tilde{r}, \hat{t})\mathrm{d}\tilde{r}$$

(we recall that $\hat{t}$ is a function of t given below eq 31 in the main text). We obtain after derivation of eq A46 with respect to time and rearrangements

$$\partial\rho_{ML}^V(t)/\partial t = Q(t)'\left[\rho_M^V - R(t) + \frac{Q(t)}{Q(t)'}(\rho_M^{V\prime} - R(t)')\right] \quad \text{(A47)}$$

where the symbol F' designates the derivative with respect to time of function F. Identification of eq A44 with eq A47 provides

$$g_3(t) \equiv Q(t)' \quad \text{(A48)}$$

and

$$g_2(t) \equiv R(t) - \frac{Q(t)}{Q(t)'}(\rho_M^V(t)' - R(t)') \quad \text{(A49)}$$

Using eq A43 gives

$$g_1(t) \equiv \frac{\rho_M^s(t) - g_2(t)}{\rho_M^V(t) - g_2(t)} \quad \text{(A50)}$$

where $\rho_M^s(t)$ and $\rho_M^V(t)$ are explicitly given by eqs A52 and A58, respectively. The $\rho_M^V(t)'$ in eq A49 may be explicitly obtained by differentiation of eq A58 with respect to time.

Appendix 4. Derivations of ρ_M^s, ρ_{ML}^V, and ρ_M^V in the Short Time Domain

A.4.1. The volume concentration ρ_M^s of free metal M over the soft shell layer of a colloidal ligand particle is written

$$\rho_M^s(\hat{t}) = \frac{4\pi r_c^2 c_M^*}{V_s}\int_0^{\tilde{d}} (\tilde{r} + \tilde{a})\xi_M(\tilde{r}, \hat{t})\mathrm{d}\tilde{r} \quad \text{(A51)}$$

which results from the combination of eqs 22, 31, and 45 for i = M. Using eqs 39 and A41, one gets after some rearrangements

$$\rho_M^s(\hat{t}) = \frac{4\pi c_M^*}{V_s}\left(\frac{r_c}{\beta(\hat{t})}\right)^2 C_4(\hat{t})\{\beta(\hat{t})\tilde{d}\cosh(\beta(\hat{t})\tilde{d}) - [1 - \beta(\hat{t})^2\tilde{a}(\tilde{a} + \tilde{d})]\sinh(\beta(\hat{t})\tilde{d})\} \quad \text{(A52)}$$

where $C_4(\hat{t})$ is provided by eq A34.

A.4.2. On the basis of eq 47 for i = ML, one easily verifies that ρ_{ML}^V is related to ρ_{ML}^s according to

$$\rho_{ML}^V(\hat{t}) = V_s c_p \rho_{ML}^s(\hat{t}) \quad \text{(A53)}$$

Using eq 33, one shows

$$\rho_{ML}^s(\hat{t}) = \frac{\tilde{k}_a\hat{t}}{1 + \tilde{k}_d\hat{t}}\rho_M^s(\hat{t}) \quad \text{(A54)}$$

so that eq A53 may be rewritten as

$$\rho_{ML}^V(\hat{t}) = V_s c_p \frac{\tilde{k}_a\hat{t}}{1 + \tilde{k}_d\hat{t}}\rho_M^s(\hat{t}) \quad \text{(A55)}$$

where $\rho_M^s(\hat{t})$ is given by eq A52.

A.4.3. The volume concentration ρ_M^V of free metal M over the unit cell of radius $a + r_c$ is given by

$$\rho_M^V(\hat{t}) = \frac{4\pi r_c^2 c_M^*}{V_c}\int_0^1 (\tilde{r} + \tilde{a})\xi_M(\tilde{r}, \hat{t})\mathrm{d}\tilde{r} \quad \text{(A56)}$$

Splitting the integral in eq A56 into a part that covers the shell layer ($0 \le \tilde{r} \le \tilde{d}$) and another which pertains to the electrolytic solution within a unit cell ($\tilde{d} \le \tilde{r} \le 1$), we find

$$\rho_M^V(\hat{t}) = \frac{V_s}{V_c}\rho_M^s(\hat{t}) + \frac{4\pi r_c^2 c_M^*}{V_c}\int_{\tilde{d}}^1 (\tilde{r} + \tilde{a})\xi_M(\tilde{r}, \hat{t})\mathrm{d}\tilde{r} \quad \text{(A57)}$$

Using eqs 38 and A32, eq A57 may be rewritten in the form

$$\rho_M^V(\hat{t}) = 4\pi c_M^* c_p \left(\frac{r_c}{\beta(\hat{t})}\right)^2 C_4(\hat{t}) h_1(\hat{t}) + c_M^* \left\{ \frac{V_c - V_p}{V_c} + 4\pi \left(\frac{r_c}{\lambda(\hat{t})}\right)^2 c_p C_1(\hat{t}) h_2(\hat{t}) \right\} \quad \text{(A58)}$$

with $C_1(\hat{t})$ is provided by eq A31 and

$$h_1(\hat{t}) = \beta(\hat{t})\tilde{d}\cosh(\beta(\hat{t})\tilde{d}) - [1 - \beta(\hat{t})^2 \tilde{a}(\tilde{a} + \tilde{d})]\sinh(\beta(\hat{t})\tilde{d}) \quad \text{(A59)}$$

$$h_2(\hat{t}) = [\lambda(\hat{t})(1 + \tilde{a})\sinh(\lambda(\hat{t})) - \cosh(\lambda(\hat{t}))] \times \left\{ \frac{\cosh(\lambda(\hat{t})\tilde{d}) - \lambda(\hat{t})(\tilde{a} + \tilde{d})\sinh(\lambda(\hat{t})\tilde{d})}{\lambda(\hat{t})(1 + \tilde{a})\sinh(\lambda(\hat{t})) - \cosh(\lambda(\hat{t}))} + \frac{\lambda(\hat{t})(\tilde{a} + \tilde{d})\cosh(\lambda(\hat{t})\tilde{d}) - \sinh(\lambda(\hat{t})\tilde{d})}{\lambda(\hat{t})(1 + \tilde{a})\cosh(\lambda(\hat{t})) - \sinh(\lambda(\hat{t}))} \right\} \quad \text{(A60)}$$

For $r_c \to \infty$ and a (necessarily small) $\hat{t}$, eqs A52, A55, and A58 simplify, taking the expressions given by eqs A39 and A42 for $C_1(\hat{t})$ and $C_4(\hat{t})$ (valid for $r_c \to \infty$), respectively, and replacing the function h_2 in eq A58 by its limit for $r_c \to \infty$, that is

$$h_2(\hat{t}) = [\cosh(\lambda(\hat{t})\tilde{d}) - \sinh(\lambda(\hat{t})\tilde{d})][1 + \lambda(\hat{t})(\tilde{a} + \tilde{d})] \quad \text{(A61)}$$

Appendix 5. Derivation of Equation 55 in the Main Text

The neglect of the polarization concentration of free metal within the particle shell leads to $\rho_M^s(t) \approx c_M(r = a + d, t)$, and eq 46 then simplifies to

$$\frac{\partial \rho_{ML}^V(t)}{\partial t} = -k_d \rho_{ML}^V(t) + k_a c_M(r = a + d, t) \rho_L^V \quad \text{(A62)}$$

Summation of eqs 4 and 5 and subsequent integration over the shell volume provides

$$\frac{\partial}{\partial t}\{\rho_{ML}^s(t) + \rho_M^s(t)\} = \frac{4\pi D_M}{V_s}(a + d)^2 \left.\frac{dc_M}{dr}\right|_{r=a+d} \quad \text{(A63)}$$

where we have used the relation

$$\int_a^{a+d} r^2 \nabla^2 c_M(r, t) dr = (a + d)^2 \left.\frac{dc_M}{dr}\right|_{r=a+d} \quad \text{(A64)}$$

Multiplying both sides of eq A63 by $c_p V_s$ and recalling that $c_p V_s \to 0$ for $r_c \to \infty$, it becomes

$$\frac{\partial \rho_{ML}^V(t)}{\partial t} \approx 4\pi(a + d)^2 D_M c_p \left.\frac{dc_M}{dr}\right|_{r=a+d} \quad \text{(A65)}$$

In the quasi-steady-state regime, the time variation of ρ_{ML}^V may be taken from the gradient of the steady-state profile of free metal just outside of the particle shell (eq 54), so that eq A65 becomes

$$\frac{\partial \rho_{ML}^V(t)}{\partial t} \approx 4\pi(a + d) D_M c_p \{c_M^* - c_M(r = a + d, t)\} \quad \text{(A66)}$$

Eliminating $c_M(r = a + d, t)$ from eq A66 and substitution in eq A62 gives

$$\frac{\partial \rho_{ML}^V(t)}{\partial t} \approx \left(1 + \frac{k_a \rho_L^V}{4\pi(a + d) D_M c_p}\right)^{-1} \left(-k_d \rho_{ML}^V(r, t) + k_a c_M^* \rho_L^V\right) \quad \text{(A67)}$$

Identification of eq A67 with eq 7 immediately gives eq 55 providing $\rho_M^V \approx c_M^*$, which is justified for very dilute colloidal ligand suspensions (as verified a posteriori from the rigorous numerical analysis of the local M concentration profiles within and outside of the particle shell as well as from the analytical developments detailed in section 2.2).

Glossary

List of Main Symbols and Abbreviations

a:	Radius of the core of the soft colloidal ligand particle (m)
$\tilde{a}$:	Normalized radius of the core of the soft colloidal ligand particle ($\tilde{a} = a/r_c$)
$c_{i=M,ML}$:	Local concentration of species i (=M, ML) within a unit cell (mol m^{-3})
$\tilde{c}_{i=M,ML}$:	Dimensionless local concentration of species i (=M, ML) within a unit cell
c_L^*:	Bulk concentration of reactive sites within the soft part (shell layer) of the colloidal ligand particle (mol m^{-3})
c_M^*:	Initial bulk concentration of free-metal species (mol m^{-3}) in the electrolytic solution
c_p:	Particle number concentration in the sample volume (m^{-3})
c^∞:	Bulk concentration of z/z background electrolyte
$C_{1,2,3,4}(\hat{t})$:	Integration constants (m) (Appendix 2)
$\vec{C}^{(k)}$:	Vector column given by eq 27
d:	Thickness of the soft layer of the colloidal ligand particle (m)
$\tilde{d}$:	Normalized thickness of the soft surface layer of the colloidal ligand particle ($\tilde{d} = d/r_c$)
D_M^{sol}:	Diffusion coefficient of free metal outside of the particle shell (m^2 s^{-1})
D_M^p:	Diffusion coefficient of free metal within the particle shell (m^2 s^{-1})
D_M ($= D_M^p = D_M^{sol}$):	Diffusion coefficient of free metal within/outside of the particle shell when its water content is sufficiently high (m^2 s^{-1})
$D_{particle}$:	Diffusion coefficient of the particle (m^2 s^{-1})
$f_{1,2,3,4}(\hat{t})$:	Functions of time defined in Appendix 2
$g_{1,2,3}(\hat{t})$:	Functions of time defined in Appendix 3
$h_{1,2}(\hat{t})$:	Functions of time defined in Appendix 4
i, k:	Integers
K:	Stability constant for the (ML) complex (mol^{-1} m^3)
k_a:	Formation rate constant of the complex (ML) (mol^{-1} m^3 s^{-1}), ($k_a = K_{os} k_w$)
k_d:	Dissociation rate constant of the complex (ML) (s^{-1})
$\tilde{k}_a$, $\tilde{k}_d$, k_{an}, k_{dn}:	Normalized formation and dissociation rate constants of the complex (ML)
k_a^*:	Generalized formation rate constant of the complex (ML) in the absence of a macroscopic consuming interface (mol^{-1} m^3 s^{-1})
k_d^*:	Generalized dissociation rate constant of the complex (ML) in the absence of a macroscopic consuming interface (s^{-1})
k_a^{**}:	Generalized formation rate constant of the complex (ML) in the presence of a

	macroscopic consuming interface (mol^{-1} m^3 s^{-1})
k_d^{**}:	Generalized dissociation rate constant of the complex (ML) in the presence of a macroscopic consuming interface (s^{-1})
K_{os}:	Stability constant of outersphere complexes (mol^{-1} m^3)
k_w:	Rate constant for water substitution (s^{-1})
L:	Ligand species
l:	Typical separation distance between neighboring reactive sites within the surface layer of the soft colloidal ligand particle
M:	Free-metal species
M:	Integer
ML:	Complex species
N:	Integer
$\vec{Q}^{(k)}$:	Vector column given by eq 28
r:	Radial position (m)
r_c:	Characteristic dimension that enters the definition of the radius of a unit cell (m)
$\tilde{r}$:	Dimensionless radial position (defined below eq 31)
t:	Time (s)
$\tilde{t}$:	Dimensionless time (used in numerical analysis)
$\hat{t}$:	Dimensionless time (used in analytical developments)
V_c:	Volume of a unit cell (m^3)
V_s:	Volume of the shell layer component of the colloidal ligand particle (m^3)
V_p:	Volume of the colloidal ligand particle (m^3)
x_p, x_s:	Dimensionless space variables (eqs 20 and 21)

Greek Symbols

$\beta(\hat{t})$:	Dimensionless function of time
ε:	Ratio D_M^p/D_M^{sol}
ϕ:	Volume fraction of soft colloidal ligand particles in the sample volume
$\xi_{i=M,ML}$:	Function of the local concentration $c_{i=M,ML}$ defined by eqs 30 and 31 (m)
$\lambda(\hat{t})$:	Dimensionless function of time
Ω:	$3M \times 3M$ sparse matrix (Appendix 1)
ψ:	Local electrostatic potential at the interface of the soft particle/electrolyte solution
ρ_i^V:	Volume concentration of species i over the spatial region of a unit cell ($mol\ m^{-3}$)
ρ_i^s:	Volume concentration of species i over the shell layer of the colloidal ligand particle ($mol\ m^{-3}$)
ρ_{fix}:	Volume charge density within the surface layer of the soft colloidal ligand particle

References and Notes

(1) Waldichuk, M. In *Pollution and Physiology of Marine Organisms.*; Vernberg, F. J., Vernberg, W. B., Eds.; Academic Press: New York, 1984.

(2) Shparyk, Y. S.; Parpan, V. I. *Environ. Pollut.* **2004**, *130*, 55.

(3) Chilrud, S. N.; Bopp, R. F.; Simpson, H. J.; Ross, J. M.; Shuster, E. L.; Chaky, D. A.; Walsh, D. C.; Choy, C. C.; Tolley, L. R.; Yarma, A. *Environ. Sci. Technol.* **1999**, *33*, 657.

(4) Ryan, J. J.; Amirova, Z.; Carrier, G. *Environ. Health Perspect.* **2002**, *110*, A699.

(5) Buffle, J. In *Complexation Reactions in Aquatic Systems. An Analytical Approach*; Ellis Horwood: Chichester, U.K., 1988.

(6) Mota, A. M.; Correia dos Santos, M. M. In *Metal Speciation and Bioavailibility*; Tessier A., Turner, D., Eds.; John Wiley and Sons: New York, 1995; Chapter 5.

(7) Davison, W. *J. Electroanal. Chem.* **1978**, *87*, 395.

(8) Van Leeuwen, H. P.; Buffle, J.; Cleven, R. *Pure Appl. Chem.* **1989**, *61*, 255.

(9) Pinheiro, J. P.; Mota, A. M.; van Leeuwen, H. P. *Colloids Surf., A* **1999**, *151*, 181.

(10) Galceran, J.; Puy, J.; Salvador, J.; Cecilia, J.; van Leeuwen, H. P. *J. Electroanal. Chem.* **2001**, *505*, 85.

(11) Galceran, J.; Puy, J.; Salvador, J.; Cecilia, J.; Mas, F.; Garces, J. L. *Phys. Chem. Chem. Phys.* **2003**, *5*, 5091.

(12) Pinheiro, J. P.; Minor, M.; van Leeuwen, H. P. *Langmuir* **2005**, *21*, 8635.

(13) Duval, J. F. L. In *Environmental Colloids and Particles: Behaviour, Separation and Characterization*; Wilkinson, K. J., Lead, J. , Eds.; John Wiley and Sons: Chichester, U.K., 2007; Vol. 10, Chapter 7.

(14) Rotureau, E.; Thomas, F.; Duval, J. F. L. *Langmuir* **2007**, *23*, 8460.

(15) Duval, J. F. L.; Slaveykova, V. I.; Hosse, M.; Buffle, J.; Wilkinson, K. J. *Biomacromolecules* **2006**, *7*, 2818.

(16) Duval, J. F. L.; Busscher, H. J.; Van de Belt-Gritter, B.; Van der Mei, H. C.; Norde, W. *Langmuir* **2005**, *21*, 11268.

(17) Morel, F. M. M.; Hering, J. G. In *Principles and Applications of Aquatic Chemistry*; John Wiley: New York, 1993.

(18) Kuwabara, S. *J. Phys. Soc. Jpn.* **1959**, *14*, 527.

(19) Stulik, K.; Amatore, C.; Holub, K.; Marecek, V.; Kutner, W. *Pure Appl. Chem.* **2000**, *72*, 1483.

(20) Buffle, J.; Horvai, G. In *In Situ Monitoring of Aquatic Systems: Chemical Analysis and Speciation*; Buffle, J., Horvai, G., Eds.; John Wiley and Sons: New York, 2000; pp 11−12.

(21) Oldham, K. B. In *Microelectrodes: Theory and Applications*; Montenegro, M.I., Queiros, M.A., Daschbach, J.L., Eds.; NATO ASI Series E 197; Kluwer: Dordrecht, The Netherlands, 1991; p 35.

(22) Yoshida, N. *J. Phys. Chem.* **1978**, *69*, 4867.

(23) Nilsson, L. G.; Nordenskiold, L.; Stilbs, P.; Braunlin, W. H. *J. Phys. Chem.* **1985**, *89*, 3385.

(24) Fatin-Rouge, N.; Milon, A.; Buffle, J.; Goulet, R. R.; Tessier, A. *J. Phys. Chem. B* **2003**, *107*, 12126.

(25) Bard, A. J.; Faulkner, L. In *Electrochemical Methods: Fundamentals and Applications*; John Wiley and Sons: New York, 2001, p 165.

(26) Pinheiro, J. P.; Galceran, J.; van Leeuwen, H. P. *Environ. Sci. Technol.* **2004**, *38*, 2397.

(27) Press, W. H.; Teukolsky, S. A.; Vetterling, W. T.; Flannery, B. P. In *Numerical Recipes in Fortran, The Art of Scientific Computing*, 2nd ed.; Cambridge University Press: New York, 1986.

(28) Qian, S.; Duval, J. F. L. *J. Colloid Interface Sci.* **2006**, *300*, 413.

(29) Singh, T.; Dutt, J. *J. Electroanal. Chem.* **1985**, *190*, 65.

(30) Compton, R. G.; Pilkington, M. B. G.; Stearn, G. M.; Unwin, P. R. *J. Electroanal. Chem.* **1987**, *238*, 43.

(31) Zhang, Z.; Buffle, J.; Alemani, D. *Environ. Sci. Technol.* **2007**, *41*, 7621.

JP709576J